POLITECNICO DI TORINO
Repository ISTITUZIONALE

Lifecycle cost optimization of tuned mass dampers for the seismic improvement of inelastic structures

Original
Lifecycle cost optimization of tuned mass dampers for the seismic improvement of inelastic structures / Matta, E.. - In: EARTHQUAKE ENGINEERING & STRUCTURAL DYNAMICS. - ISSN 0098-8847. - STAMPA. - 47:3(2018), pp. 714-737. [10.1002/eqe.2987]

Availability:
This version is available at: 11583/2702989 since: 2020-05-11T09:57:52Z

Publisher:
John Wiley and Sons Ltd

Published
DOI:10.1002/eqe.2987

Terms of use:

This article is made available under terms and conditions as specified in the corresponding bibliographic description in the repository

Publisher copyright
Wiley postprint/Author's Accepted Manuscript

This is the peer reviewed version of the above quoted article, which has been published in final form at http://dx.doi.org/10.1002/eqe.2987.This article may be used for non-commercial purposes in accordance with Wiley Terms and Conditions for Use of Self-Archived Versions.

(Article begins on next page)

26 November 2026

Lifecycle cost optimization of tuned mass dampers for the seismic improvement of inelastic structures

E. Matta [1*]

[1] Politecnico di Torino, Corso Duca degli Abruzzi 24, Turin, Italy
[*] E-mail: emiliano.matta@polito.it · Phone: +39 011 090 4867 · ORCID: 0000-0001-5453-1470

Abstract The seismic performance of tuned mass dampers (TMDs) on structures undergoing inelastic deformations may largely depend on the ground motion intensity. By estimating the impact of each seismic intensity on the overall cost of future seismic damages, lifecycle cost (LCC) proves a rational metric for evaluating the benefits of TMDs on inelastic structures. However, no incorporation of this metric into an optimization framework is reported yet. This paper presents a methodology for the LCC-optimal design of TMDs on inelastic structures, which minimizes the total seismic LCC of the combined building-TMD system. Its distinctive features are the assumption of a mass-proportional TMD cost model, the adoption of an iterative sub-optimization procedure and the initialization of the TMD frequency and damping ratios according to a conventional linear TMD design technique. The methodology is applied to the seismic improvement of the SAC-LA benchmark buildings, taken as representative of standard steel moment-resisting-frame office buildings in LA, California. Results show that, despite their limited performance at the highest intensity levels, LCC-optimal TMDs considerably reduce the total LCC, to an extent which depends on both the building vulnerability and the TMD unit cost. They systematically present large mass ratios (around 10%) and frequency and damping ratios close to their respective linearly designed optima. Simulations reveal the effectiveness of the proposed design methodology and the importance of adopting a nonlinear model in order to correctly evaluate the cost-effectiveness of TMDs on ordinary structures in highly seismic areas.

Keywords Lifecycle cost (LCC) · Tuned mass damper (TMD) · Optimal design · Inelastic structures · Seismic improvement

1 Introduction

Among the several vibro-protecting strategies recently developed to improve safety and serviceability of civil structures under dynamic loads, passive tuned mass dampers (TMDs) have been broadly investigated and applied on both new and existing structures [1]. In its basic configuration, a TMD is a single-degree-of-freedom (SDOF) mass-spring-dashpot system appended to the main structure. By tuning the TMD frequency to the frequency of the structural target mode and by optimizing the TMD damping, a dynamic interaction is established between the target mode and the TMD, through which a significant amount of vibratory energy is transferred from that mode to the TMD and eventually dissipated [2].

Widely used to reduce the response of flexible low-damped structures to quasi-stationary dynamic loads, TMDs are less frequently employed for the seismic improvement of buildings, where their effectiveness is still a debated issue. As the main structure remains linear, a satisfactory performance is generally acknowledged [3-6], which is greater against long-duration, narrow-band ground motions, but acceptable even against impulsive earthquakes if large mass ratios are used [7-9]. On nonlinear structures, however, TMDs' seismic effectiveness is more controversial. Analysing TMDs on single- and multi-storey inelastic structures, several researches in the 1980s and 1990s report insignificant reductions of peak displacements and accelerations under high-intensity ground motions [10-14]. Looking at the peak reduction as an insufficient criterion, more recent studies emphasize TMDs' ability to reduce low-cycle fatigue damage in the event of medium-intensity earthquakes [15-19]. As a result, TMDs are currently considered a successful control strategy under moderate earthquakes, i.e. when the structure remains linear or weakly nonlinear, but scarcely effective or even detrimental under severe ground shaking, i.e. when the structural response turns highly nonlinear. Conventional methods for evaluating representative engineering demand parameters (EDPs), such as peak response or energy reduction indices, cannot provide a concise measure of this trade-off between seismic amplitude and TMD effectiveness, since they cannot weigh, on a sound economic basis, the relative significance of different intensity levels. Alternatively, a comprehensive probabilistic lifecycle cost (LCC) evaluation should be adopted, reflecting how moderate and severe earthquakes respectively contribute to the expected cost of future damages and losses. Complemented with an estimation of the TMD investment cost, LCC analysis can provide a rational and reliable measure of TMD cost-effectiveness, directly expressed in monetary units and immediately useable by asset managers. By adopting an LCC approach, investors and managers, instead of merely looking at an asset in terms of costs to design and build (initial cost), can broaden their perspective by including all operation, maintenance, repair, replacement and disposal costs over a period

of time (lifetime cost). The sum of the initial and the lifetime costs determines the total LCC of the system. Its minimization should be the primary objective of any design process, either in building new constructions or in retrofitting existing ones.

LCC evaluation and design have been increasingly applied to seismic engineering in the last decades [20-23], particularly to the area of passive [24-25] and semi-active [26] structural control. More recently, LCC concepts have also been applied to TMDs, generally assuming a linear structural behaviour. In [27] an integrated performance-based optimization is proposed for the design of a semi-active TMD on a tall linear building structure under wind loads; the goal is to minimize the LCC of the overall system, including the initial and lifetime costs of both the building and the control system. In [28] different retrofitting strategies, including nonlinear dissipative bracings and traditionally optimized TMDs, are simulated on a tall linear building structure under wind action, and compared in terms of investment costs and conventional performance measures. In [29] a multi-objective LCC optimization is applied to TMDs and tuned liquid dampers (TLDs) on linear building structures exposed to typical Chilean long-duration, far-field earthquakes, proving that TMDs are cost-effective for the Chilean region, and TLDs are even more because of their lesser construction and maintenance cost. In [30] a multi-objective optimization of a TMD on a linear building structure under moderate seismic loading is proposed, aimed at minimizing both the structural acceleration and a linear combination of the TMD parameters (mass, stiffness and damping coefficient) intended as a measure of the TMD cost. On the other hand, the very few studies dealing with TMDs on nonlinear structures do not attempt an LCC optimization. In [31] a comprehensive robust stochastic optimization of TMDs on nonlinear structures is presented, but the design objective is actually system reliability, and no cost-related issues are considered. In [32] a parametric investigation of the LCC of a Bouc-Wen hysteretic SDOF building structure equipped with a TMD is presented, but the TMD is optimized in a traditional way and its cost is excluded from the analyses. In [33] a methodology for evaluating the seismic LCC-effectiveness of TMDs on inelastic building structures is proposed, but the TMD mass is *a-priori* assigned and no LCC optimization is attempted. In summary, to the best of the author's knowledge, no LCC-optimal strategy for designing TMDs on inelastic structures has ever been reported in the literature.

To bridge the gap, a methodology is proposed in this paper to perform the LCC-optimal design of TMDs on standard building structures exposed to seismic hazard, exhibiting an inelastic response under high intensity ground motions. The objective of the methodology is not to achieve a code-compliant seismic retrofit, i.e. to satisfy conventional constraints imposed by pre-determined normative requirements (as in classical performance-based design), but rather to minimize the total LCC of the overall building-TMD system, so as to ensure the most cost-effective seismic improvement of the existing building. In principle, this approach cannot prevent the optimal solution from largely exceeding, at least at a local scale, the structural damage constraints usually prescribed to new constructions. However, imposing strict local constraints is *per se* hardly compatible with a TMD design, particularly for applications on existing structures, because TMDs can improve the structural response globally, but have scarce capability to selectively affect it at specified locations. On the other hand, this also ensures that no significant worsening of the local response will occur as the result of TMD installation. With this in mind, if the retrofit aims at dramatically resolving severe local inadequacies, a TMD is likely not the right solution. In all the other cases, the LCC methodology proposed in this paper is a viable design option. In what follows, its theoretical framework is detailed in Section 2 while an application is illustrated in Section 3. Conclusions are drawn in Section 4.

2 LCC-optimal seismic design of TMDs on inelastic building structures

2.1 Premise

In the last decades, several methodologies have been developed for the optimal design of civil structures considering, explicitly or implicitly, their lifecycle cost performance. In [34] the optimal design of bridge maintenance scheduling is discussed and the LCC performance is estimated using a general reliability framework. In [35] reinforced concrete buildings are analysed and repair costs are described for each level of ground motion intensity using a global Park-Ang damage index. In [36] the LCC-optimal seismic design of steel frame buildings is performed using pushover analysis. A similar methodology for estimating repair losses is adopted in [37]. In [24] a complete probabilistic framework is presented for the optimization of the LCC performance of engineering systems, based on nonlinear dynamic analyses and focused on the design of passive dissipative devices.

The main goal of this paper is the formulation of an LCC optimization methodology for the seismic design of TMDs on multi-degree-of-freedom (MDOF) inelastic building structures. To this purpose, an LCC

performance evaluation criterion must be established first. Among the several available methods, the one developed in [38] and subsequently improved by Lagaros and co-authors [39-41] appears particularly appealing for its simplicity, and is adopted here with only slight variations. It makes damage and consequently lifetime cost depend on one or more seismic EDPs, evaluated at multiple intensity levels through static or dynamic nonlinear analyses. Because simulating the structure-TMD interaction requires time-domain analyses, the variant operating in the dynamic domain is herein chosen. Based on this criterion, the new LCC design methodology is presented in this Section. Although its general framework is also applicable to new constructions, the main focus is here on the seismic improvement of existing structures, intended as completely assigned and excluded from the optimization process.

2.2 Analytical model of an inelastic building with TMD

Large magnitude earthquakes can inflict severe damages to civil structures, resulting in highly nonlinear structural responses. In this study, inelastic MDOF steel moment-resisting-frame (MRF) building structures equipped with single linear passive TMDs are simulated under seismic loading. For simplicity, analysis is restricted to planar (2D) models. Without loss of generality, material nonlinearity is assumed to be concentrated in the inelastic hinges placed at the ends of the structural members. A bilinear hardening-type hysteretic model is adopted for the inelastic hinges, while a linear elastic model is assumed for the structural members. A lumped mass formulation is adopted for representing the inertial forces. The TMD is modelled as a linear SDOF mass-spring-dashpot system, attached to the top storey and tuned to the fundamental structural mode (target mode).

Condensed to the horizontal degrees of freedom of the structural frame, the equations of motion for the 2D model of an N_S-storey inelastic MRF structure, coupled with a TMD located atop and subjected to a ground acceleration input, can be written as follows (Figure 1):

$$\mathbf{M}\ddot{\mathbf{u}} + \mathbf{C}\dot{\mathbf{u}} + \mathbf{f}_{\mathrm{r}} + \mathbf{f}_{\mathrm{P\text{-}\Delta}} = -\mathbf{M}\mathbf{t}_g\ddot{u}_g + \mathbf{t}_p p \tag{1}$$

$$m_T\ddot{u}_T + p = -m_T\ddot{u}_g \tag{2}$$

with

$$p = c_T(\dot{u}_T - \dot{u}_{N_S}) + k_T(u_T - u_{N_S}) \tag{3}$$

$$\mathbf{f}_{\mathrm{P\text{-}\Delta}} = -\mathbf{P}\boldsymbol{\theta} = -\mathbf{P}\mathbf{T}\mathbf{u} = \mathbf{K}_{\mathrm{P\text{-}\Delta}}\mathbf{u} \tag{4}$$

where:

$\mathbf{u} = [u_1 \;\; u_2 \;\ldots\; u_{N_S}]^T$ is the horizontal displacement vector of the structure relative to the ground;

$\mathbf{M}$ and $\mathbf{C}$ are, respectively, the mass and the damping matrices of the structure;

$\mathbf{f}_{\mathrm{r}}$ is the lateral restoring force vector;

$\ddot{u}_g$ is the ground acceleration;

$\mathbf{t}_g = [1 \;\; 1 \;\ldots\; 1]^T$ is the topological vector related to the ground acceleration;

p is the TMD reaction force;

$\mathbf{t}_p = [0 \;\ldots\; 0 \;\; 1]^T$ is the topological vector related to the TMD reaction force;

u_T is the horizontal displacement of the TMD relative to the ground;

m_T, c_T and k_T are the mass, damping and stiffness coefficients of the TMD;

$\mathbf{f}_{\mathrm{P\text{-}\Delta}}$ is the P-delta force vector accounting for the second-order effects;

$\mathbf{P}$ is the P-delta cumulative gravity load matrix computed from the mass of the structure-TMD system and the acceleration of gravity g as follows:

$$\mathbf{P}(i,i) = g\left[\left(\sum_{j=i}^{N_S}\mathbf{M}(j,j)\right) + m_T\right], \quad \forall i = 1,2,...,N_S$$

$$\mathbf{P}(i-1,i) = -\mathbf{P}(i,i), \quad \forall i = 2,3,...,N_S$$

$\boldsymbol{\theta} = [\theta_1 \;\; \theta_2 \;\ldots\; \theta_{N_S}]^T$ is the inter-storey drift ratio vector;

$\mathbf{T}$ is the rotation matrix, transforming the displacement vector $\mathbf{u}$ into the inter-storey drift ratio vector $\boldsymbol{\theta}$;

$\mathbf{K}_{\mathrm{P\text{-}\Delta}} = -\mathbf{P}\mathbf{T}$ is the geometric stiffness matrix accounting for P-delta effects.

The restoring force vector $\mathbf{f}_r$ results from the equilibrium of all internal forces and moments at the members' ends, expressed as a function of the generalized displacements of every structural node [42]. The P-delta force vector $\mathbf{f}_{P\text{-}\Delta}$ accounts for the second-order effects caused by the cumulative gravity loads [43]. These effects may be significant for steel MRF structures, usually flexible and prone to large lateral displacements under seismic loading. The addition of a TMD further increases the cumulative gravity loads, augmenting the P-delta effects. As a consequence of the P-delta effects, the lateral load resistance of the i^{th} storey is approximately reduced by $\mathbf{P}(i,i)\theta_i$, and the lateral stiffness of the frame structure is accordingly reduced by the **PT** term defined above. Eqs. (1) to (4), once reformulated in an incremental form, can be solved, for instance, by using the Newmark-β time-step integration method [42].

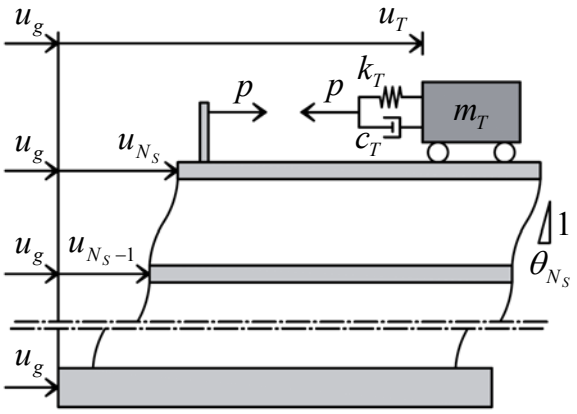


Figure 1. Schematics of the 2D model of an N_S-storey MRF structure with a TMD atop.

As long as the structure responds in its linear elastic range, the restoring force vector can be expressed as $\mathbf{f}_r = \mathbf{K}_e\mathbf{u}$ and Eq. (1) can be linearized as follows:

$$\mathbf{M}\ddot{\mathbf{u}} + \mathbf{C}\dot{\mathbf{u}} + \mathbf{K}\mathbf{u} = -\mathbf{M}\mathbf{t}_g\ddot{u}_g + \mathbf{t}_p p \tag{5}$$

where:

$\mathbf{K}_e$ is the elastic stiffness matrix of the structure, excluding second-order effects;

$\mathbf{K} = \mathbf{K}_e + \mathbf{K}_{P\text{-}\Delta}$ is the total stiffness matrix of the structure, including second-order effects.

For the linearized system in Eq. (5), classical input-output transfer functions (TFs) can be computed, traditionally adopted in TMD design. The same TFs, as will be shown in Section 2.4, can be profitably used in an LCC context even when the fully nonlinear model in Eqs. (1) to (4) holds.

2.3 LCC performance evaluation of an inelastic building with TMD

2.3.1 Evaluation of the EDP

In earthquake engineering, LCC analysis requires the calculation of cost components related to the performance of the structure in multiple levels of seismic intensity. To this purpose, incremental static or dynamic analyses can be incorporated into the LCC assessment methodology [44]. One of the most successful multi-level LCC methods implementing nonlinear dynamic analysis is the multiple-stripe dynamic analysis (MSDA). In MSDA, different suites of nonlinear dynamic analysis (stripes) are performed. Each suite corresponds to a given seismic intensity level, i.e. to a predetermined exceedance probability in a given time period, according to the seismic hazard curve at the site. As a result, a correlation is established between the seismic intensity, expressed by a proper intensity measure (IM), and the corresponding structural response, described by an appropriate EDP. Because of the high computational effort required by 3D analyses, 2D simulations are usually preferred.

Selecting the appropriate IM and EDP is paramount in MSDA. The IM is typically chosen as a monotonically scalable ground motion parameter, such as the peak ground acceleration or the 5%-damped spectral acceleration at the fundamental structural period. On the other hand, various EDPs are available [45], among which the storey drift demand, expressed by the peak inter-storey drift ratio θ, is by far the most frequently adopted [43]. In fact, established relations exist between θ and performance-oriented descriptions such as immediate occupancy, life safety and collapse prevention [46], as well as between θ and damage, for both reinforced concrete [47] and steel frame structures [38]. θ is also recommended by FEMA-350 [48] as the most

suitable performance criterion for frame structures. In this paper, MSDA is chosen as the LCC evaluation criterion, and is applied to the 2D mechanical model presented in Section 2.2 by considering $N_L = 7$ intensity levels, each described by a suite of $N_R = 10$ two-components spectrum-compatible records. On the other hand, θ is here chosen as the only significant EDP, and the relation between θ and damage is taken as proposed for steel MRF structures by [38], articulated in the $N_D = 7$ damage states defined in Table 1. More specifically, for every storey, the EDP representing a given intensity level (i.e. a given set of records), denoted as set-EDP, is computed as follows: (i) first, for every record in that set, a nonlinear analysis is separately performed under both its components, and the largest of the two θs is taken as the record-EDP; (ii) then, the mean value of all record-EDPs contained in that set is taken as the corresponding set-EDP.

Table 1 Damage states as a function of the peak inter-storey drift ratio [38]

Damage state	Peak inter-storey drift ratio θ (%)
1-None	$0.0 \le \theta < 0.2$
2-Slight	$0.2 \le \theta < 0.5$
3-Light	$0.5 \le \theta < 0.7$
4-Moderate	$0.7 \le \theta < 1.5$
5-Heavy	$1.5 \le \theta < 2.5$
6-Major	$2.5 \le \theta < 5.0$
7-Destroyed	$5.0 \le \theta$

Although a significant damage indicator for acceleration-sensitive non-structural components, structural acceleration is not taken here, instead, as an additional EDP. As in many recent LCC studies (e.g. [37], [39], [40], [44]), the damage cost of all non-structural components is here related to the drift ratio only, with no distinction between drift-sensitive and acceleration-sensitive components. Considering the LCC of low-rise office buildings in highly seismic regions, Taflanidis and Beck [24] show that the relative contribution of acceleration-sensitive contents to the overall lifetime damage cost is practically negligible. Optimizing a single TMD on a 10-storey linear building structure, Lavan [49] confirms that displacements and accelerations are substantially not competing objectives in TMD optimal design. Not specifically accounting for acceleration-related damage, the LCC formulation herein adopted may lead to a certain underestimation of damage cost especially in the case of tall buildings, for which the relative significance of accelerations with respect to inter-storey drift ratios increases. This underestimation, which mainly implies a slight underestimation of the TMD cost-effectiveness, is however expected to negligibly affect the TMD design process. Further investigations on this issue are anyway left for future work.

2.3.2 LCC model for a structure with TMD

The expected LCC of a structure-TMD system over the lifetime period t, which may be the design life of a new structure or the remaining life of an existing one, can be given as follows [38-39]:

$$C_{TOT} = C_{IN,S} + C_{DS,S} + C_{IN,T} + C_{DS,T} \tag{6}$$

where $C_{IN,S}$ and $C_{IN,T}$ are the initial costs of, respectively, the structure and the TMD, and $C_{DS,S}$ and $C_{DS,T}$ are the present value of the expected costs of future seismic damages suffered, over the lifetime period t, by respectively the structure and the TMD. In particular, $C_{IN,S}$ (building initial cost) comprises the material and labour costs required for the construction of a new building or for the retrofitting of an existing one, including structural and non-structural components. $C_{IN,T}$ (TMD initial cost) comprises the costs required for the design, construction and installation of the TMD. $C_{DS,S}$ (building damage cost) comprises the cost of structural and non-structural repair, the cost of loss of contents, the cost of injury recovery or human fatality and other direct or indirect economic losses (e.g. rental and income costs). $C_{DS,T}$ (TMD damage cost) accounts for the loss of the TMD in the event of a building collapse, under the assumption that no other significant damage can afflict a conservatively designed TMD. The costs for the ordinary maintenance of, respectively, the building and the TMD are supposed to be included in $C_{IN,S}$ and $C_{IN,T}$, for simplicity.

Of the four cost components in Eq. (6), $C_{IN,S}$ is the only one being unaffected by the TMD design. Indeed, because the structure is supposed to be unchangeable in this paper, $C_{IN,S}$ is a constant term. Subtracting $C_{IN,S}$ from C_{TOT}, the "controllable" lifecycle cost C can be conveniently introduced as

$$C = C_{TOT} - C_{IN,S} = C_{DS,S} + C_{IN,T} + C_{DS,T} \tag{7}$$

obtained by summing up the expected building damage cost and the overall costs of the TMD. For a controlled structure-TMD system, minimizing C leads to the LCC-optimal TMD. For a conventional structure with no TMD, C degenerates into the uncontrolled building damage cost, denoted as C_{unc}. The more C decreases with

respect to C_{unc}, the more cost-effective the TMD is. The minimization of C will be the object of Section 2.4. The evaluation of its three cost components is detailed as follows.

2.3.3 Evaluation of the building damage cost

Considering N_D possible building damage states, the cost of the i^{th} state can be given as follows [41]:

$$C_{DS,S}^{i} = C_{dam}^{i} + C_{con}^{i} + C_{ren}^{i} + C_{inc}^{i} + C_{inj}^{i} + C_{fat}^{i} \tag{8}$$

where C_{dam}^{i} is the damage repair cost, C_{con}^{i} is the loss of contents cost, C_{ren}^{i} is the loss of rental cost, C_{inc}^{i} is the income loss cost, C_{inj}^{i} is the injury cost and C_{fat}^{i} is the human fatality cost. Details on the evaluation of each damage state cost are given in Table 2 [40], where the basic costs (third column) represent the first component of the calculation formulas (second column). The damage state parameters recalled in the calculation formulas (i.e. "mean damage index", "loss of function index", "down time index", "expected minor injury rate", "expected serious injury rate", and "expected death rate") are derived from [41] and reported, as a function of the damage state, in Table 3.

Table 2 Damage state cost calculation formulas [40]

Cost category	Calculation formula	Basic cost
Damage repair	Replacement cost x floor area x mean damage index	1500 €/m^2
Loss of content	Unit content cost x floor area x mean damage index	500 €/m^2
Rental	Rental rate x gross leasable area [(ii)] x disruption period [(iii)] x loss of function index	10 €/month/m^2
Income	Income rate x gross leasable area [(ii)] x disruption period [(iii)] x down time index	2000 €/year/m^2
Minor injury	Minor injury cost per person x floor area x occupancy rate [(i)] x expected minor injury rate	2000 €/person
Serious injury	Serious injury cost per person x floor area x occupancy rate [(i)] x expected serious injury rate	$2 \cdot 10^4$ €/person
Human fatality	Death cost per person x floor area x occupancy rate [(i)] x expected death rate	$2.8 \cdot 10^6$ €/person

[(i)] Occupancy rate: 2 persons/100 m^2; [(ii)] Gross leasable area: 90% of the total floor area; [(iii)] Disruption period: 6 months.

Based on a Poisson model of earthquake occurrences and on the assumption that damaged buildings are immediately restored to their original intact conditions after each significant seismic attack, the building damage cost $C_{DS,S}$ in Eq. (7) can be computed [38] as:

$$C_{DS,S} = \nu \left(\frac{1 - e^{-\lambda t}}{\lambda} \right) \sum_{i=1}^{N_D} C_{DS,S}^{i} P_o^{i} \tag{9}$$

where: P_o^{i} is the probability of occurrence of the i^{th} damage state given the occurrence of a significant earthquake; ν is the mean frequency of occurrence of significant earthquakes; and λ is the momentary discount rate, which actualizes future costs to their current value. Denoting the ratio in parentheses, which tends to t as λ tends to 0, as the actualized time period t_a, Eq. (9) can be more clearly rewritten as:

$$C_{DS,S} = t_a \sum_{i=1}^{N_D} C_{DS,S}^{i} \phi_o^{i} \tag{10}$$

where $\phi_o^{i} = \nu P_o^{i}$ is the mean frequency of occurrence of the i^{th} damage state. Following [38], the i^{th} damage state is identified by the peak drift ratio bounds reported in the second column of Table 1.

Table 3 Damage state parameters for cost evaluation [41]

Damage state	Mean damage index (%)	Loss of function index (%)	Down time index (%)	Expected minor injury rate	Expected serious injury rate	Expected death rate
1-None	0	0	0	0	0	0
2-Slight	0.5	0.9	0.9	$3.0 \cdot 10^{-5}$	$4.0 \cdot 10^{-6}$	$1.0 \cdot 10^{-6}$
3-Light	5	3.33	3.33	$3.0 \cdot 10^{-4}$	$4.0 \cdot 10^{-5}$	$1.0 \cdot 10^{-5}$
4-Moderate	20	12.4	12.4	$3.0 \cdot 10^{-3}$	$4.0 \cdot 10^{-4}$	$1.0 \cdot 10^{-4}$
5-Heavy	45	34.8	34.8	$3.0 \cdot 10^{-2}$	$4.0 \cdot 10^{-3}$	$1.0 \cdot 10^{-3}$
6-Major	80	65.4	65.4	$3.0 \cdot 10^{-1}$	$4.0 \cdot 10^{-2}$	$1.0 \cdot 10^{-2}$
7-Destroyed	100	100	100	$4.0 \cdot 10^{-1}$	$4.0 \cdot 10^{-1}$	$2.0 \cdot 10^{-1}$

Denoting as θ^{i} the lower bound for to the i^{th} damage state, ϕ_o^{i} in Eq. (10) is computed as:

$$\phi_o^{i} = \phi_e^{i} - \phi_e^{i+1} \tag{11}$$

where ϕ_e^{i} is the mean frequency of exceedance of θ^{i} and can be expressed by a relation of the form:

$$\phi_e^i = f(\theta^i) \tag{12}$$

Such relation is deduced by fitting a properly shaped function f to N_L known $\phi_e^j - \theta^j$ pairs, each pair corresponding to a specific intensity level characterized by a known probability of exceedance $P_{e/\tau}^j$ in a given time period τ [39]. For each pair, i.e. for each of the N_L intensity levels, the drift ratio θ^j is computed through nonlinear dynamic analyses as the set-EPS (as explained in Section 2.3.1), while the mean frequency of exceedance of θ^j, denoted as ϕ_e^j, is derived, according to Poisson's law, as:

$$\phi_e^j = -\frac{1}{\tau}\ln(1 - P_{e/\tau}^j) \tag{13}$$

After considering various alternative functional forms, f in Eq. (12) is taken as follows [33]:

$$f(\theta) = \begin{cases} \alpha_1 \theta^{-\beta_1} & for\ \theta < \theta^2 \\ \gamma(\alpha_j \theta^{-\beta_j}) + (1-\gamma)(a_j \theta + b_j) & for\ \theta^j \le \theta < \theta^{j+1},\ j = 2,...,N_H - 2 \\ \alpha_{N_L-1} \theta^{-\beta_{N_L-1}} & for\ \theta \ge \theta^{N_L-1} \end{cases} \tag{14}$$

where: α_j and β_j are analytically determined so that the hyperbolic expression $\alpha_j \theta^{-\beta j}$ exactly interpolates pairs j and j+1; a_j and b_j are analytically determined so that the linear expression $a_j\theta + b_j$ exactly interpolates pairs j and j+1; and the weight factor γ is numerically determined so that the sum of the changes of slope of $f(\theta)$ at every θ^j, expressed by $\sum_{j=2}^{N_L-1} \left| f'_+(\theta^j) - f'_-(\theta^j) \right|$, is minimum. As a result, Eq. (14) ensures a function passing through all the available N_L pairs. A graphical representation of the function f will be given later, in Figure 5.

Unlike in previous works [38-39], where the drift ratio θ is taken as the largest along the building height, here damage and cost at every storey are assumed to depend on the drift ratio measured at that storey; the global building cost then follows, computed as the summation of all the storey-level costs. The only exception are the costs related to the collapse damage state ("7-Destroyed"), still assumed to be governed, for all the storeys, by the largest θ along the building height, because the collapse of any single storey is assumed to involve the collapse of the entire building. With respect to previous studies, the slight increase in complexity of this variant is largely repaid by the improved accuracy of the cost estimation, especially in the case when most damage is localized in few storey levels.

2.3.4 Evaluation of the TMD initial cost

Few TMD cost models exist in the literature. In [24] the lack of appropriate TMD cost models is recognized as a severe impediment to the economic evaluation of TMDs' seismic performance. In [28], based on the estimations provided by two accredited Chinese construction companies, the total cost (including design, construction, installation and maintenance) of a 700 ton passive translational TMD is reported to vary between 0.75 M$ (i.e. 1070 $/ton) and 0.96 M$ (i.e. 1370 $/ton). In [29] the cost of a unidirectional passive translational TMD is assumed to be mass-proportional, with a unit cost of 2500 $/ton. In [30] a linear combination of the TMD mass, stiffness and damping parameters is introduced as an index of TMD cost, but no monetary quantification is provided.

The limited literature on this topic reflects the unconventional character of TMDs' applications and advocates the development of more accurate TMD cost models for the future.
In this paper, a proportional dependence of TMD initial cost on TMD mass is adopted, expressed by:

$$C_{IN,T} = c_U \cdot m_T \tag{15}$$

where the unit cost c_U is assumed to vary between a lower value c_{UL} = 1250 €/ton and an upper value c_{UU} = $2 \cdot c_{UL}$ = 2500 €/ton. This relation, although unable to accurately describe a specific TMD technology, is in agreement with the aforementioned literature and is general enough to fit in the present paper. It might be argued that cost-mass proportionality, not accounting for a fixed cost term, would underestimate the costs of TMDs characterized by very small mass ratios. Section 3 will show that the domain of small mass ratio is of little interest within the case studies examined in this paper, so that the said proportionality can be herein accepted. It might also be argued that Eq. (15) does not account for the dependence of the TMD initial cost on the TMD stroke demand, although the latter may play an important role in TMD optimization, sometimes even making a TMD design unfeasible (e.g. [49] and [50]). This is mainly due to the unavailability, in the literature, of explicit relations between the TMD initial cost and the TMD stroke demand, as well as of general criteria

for deriving the maximum TMD stroke capacity, still being problem-dependent. It should be added that, as long as a large TMD mass ratio is used, the optimal TMD damping ratio is typically large enough to ensure a small TMD stroke demand [8]. Further reductions can be obtained by increasing the TMD damping ratio beyond its optimal value, with the obvious inconvenient of augmenting the dashpots' cost. In the absence of TMD cost models rigorously accounting for these issues, TMD optimization is conducted in this paper without explicit consideration of TMD stroke demands, whose extent is nonetheless reported and discussed in Section 3 for the examined case studies.

2.3.5 Evaluation of the TMD damage cost

Assuming that the TMD shall be effective and undamaged as long as the building structure avoids collapse, the TMD damage cost $C_{DS,T}$ is merely the cost of losing the TMD in the event of structural collapse, and can be evaluated as follows, in analogy with Eq.(10):

$$C_{DS,T} = t_a \sum_{i=1}^{N_D} C_{DS,T}^{i} \phi_o^i = t_a C_{dam,T}^{N_D} \phi_o^{N_D} = t_a C_{IN,T} \phi_o^{N_D} \tag{16}$$

where the only nonzero damage state in the summation is the TMD damage repair cost $C_{dam,T}^{N_D}$, corresponding to the collapse damage state ($i = N_D = 7$) and here assumed to coincide with the TMD initial cost $C_{IN,T}$. Recalling Eqs. (6) and (16), the following expression for the total TMD lifecycle cost can be derived:

$$C_T = C_{IN,T} + C_{DS,T} = (1 + t_a \phi_o^{N_D}) C_{IN,T} \tag{17}$$

Because the product $t_a \phi_o^{N_D}$, expressing the probability of collapse in the period t_a, is much smaller than unity, $C_{DS,T}$ is almost negligible and C_T nearly coincides with $C_{IN,T}$.

2.4 LCC optimal design of a TMD on an inelastic building

In Section 2.3, a method for evaluating the controllable lifecycle cost C of an assigned inelastic structure equipped with an assigned TMD is established. In this Section, a method is presented to choose the TMD parameters which make C minimum. The method starts with a preliminary linear H_∞^f-design optimization, described in Section 2.4.1, and develops through an iterative three-stage procedure, detailed in Section 2.4.2.

2.4.1 The preliminary H_∞^f design

Various conventional optimization techniques are applicable to the seismic design of TMDs on linear structures. Many of these techniques intend optimality as the minimization of an appropriate norm of some input-output transfer function (TF) of the combined structure-TMD system, such as the H_2-norm [7] or the H_∞-norm [11,16]. In these cases, denoting by m_S the total mass of the uncontrolled structure, by ω_S and ζ_S the circular frequency and the damping ratio of the uncontrolled target mode, and by m_T, ω_T and c_T the mass, circular frequency and damping coefficient of the TMD, the design problem is usually posed as follows: first, the mass ratio $\mu = m_T / m_S$ is chosen by the designer, based on cost-benefit expectations; then, the optimal frequency ratio $r = \omega_T / \omega_S$ and damping ratio $\zeta = c_T / (2 \omega_T m_T)$ are determined which make the TF norm minimum.

In this study, one of these techniques is used to provide the starting point for the LCC optimization. The chosen technique is the H_∞^f design proposed in [8], consisting in the numerical minimization of the H_∞-norm of a pre-established TF, multiplied by a Kanai-Tajimi filter KT having circular frequency $\omega_g = \omega_S$ and damping ratio $\zeta_g = 0.3$. This methods is preferred over other conventional methods because it leads to a slightly improved TMD performance in the case of linear structures. The TF is here taken as the one from the ground acceleration to the maximum (along the building height) inter-storey drift ratio, denoted as $T_{\theta u}$ and computed by using the linearized structural model expressed by Eq.(5). Its Kanai-Tajimi filtered counterpart is computed as $T_{\theta u}^f = T_{\theta u} \cdot KT$.

As a preliminary step towards LCC optimization, the H_∞^f design is used to provide, for any possible value of μ, the pair of H_∞^f-optimal frequency and damping ratios, $r_{opt,H}$ and $\zeta_{opt,H}$, to be subsequently adjusted during the iteration process. In formulas:

$$R_{opt,H}(\mu) = \min_{r,\varsigma} \left\| T_{\theta u}^f(\mu, r, \varsigma) \right\|_\infty \tag{18}$$

and

$$[r_{opt,H}(\mu), \varsigma_{opt,H}(\mu)] = \arg\min_{r,\varsigma} \left\| T_{\theta u}^f(\mu, r, \varsigma) \right\|_\infty \tag{19}$$

where $R_{opt,H}(\mu)$ denotes the H_∞^f-optimal norm of the chosen TF.

2.4.2 The iterative LCC optimization

With the controllable lifecycle cost C defined by Eq. (7), the LCC-optimal TMD design can be formulated as the following constrained nonlinear 3-dimensional (3D) minimization problem:

$$C_{opt}(t) = \min_{\mu,r,\varsigma} C(\mu, r, \varsigma; t), \quad \mu \le \mu_{\max} \tag{20}$$

$$[\mu_{opt}(t), r_{opt}(t), \varsigma_{opt}(t)] = \arg\min_{\mu,r,\varsigma} C(\mu, r, \varsigma; t), \quad \mu \le \mu_{\max} \tag{21}$$

where C is the objective function, μ, r and ζ are the three design variables, and $\mu_{\max}$ is the maximum allowable TMD mass ratio, depending on static, architectural and constructive constraints.

The problem can be solved by using a variety of optimization algorithms. Because of the high computational cost of each evaluation of C, a simplified sub-optimal iterative procedure is here suggested which, although not generally ensuring the convergence to a formal optimum, yet allows, in all the examined case studies, the identification, through a limited number of evaluations, of a nearly-optimal solution, practically indistinguishable from the exact one.

The procedure is formalized by Eqs. (22) to (27). Starting from the results of an H_∞^f design, it evolves through successive iterations, with three stages in each iteration. Eqs. (22) to (24) refer to Iteration 1, Eqs. (25) to (27) to any subsequent Iteration k. In each iteration, the 3D optimization problem defined by Eqs. (20) and (21) (i.e. dependent on three design variables) is decomposed into a series of three 1D optimization problems (i.e. each dependent on a single design variable only), one for each stage. The three stages in each iteration are hierarchically ordered according to the sensitivity of the objective function to each variable, in descending order from μ to ζ. The procedure is initialized (Iteration 1 - Stage 1) to the results of an H_∞^f design: Eq. (22) indeed spans the μ domain in search of the minimum C (an example will be given later in Figure 6), under the assumption that r and ζ are taken as the corresponding H_∞^f-optimal values (in some analogy to the multiple TMD design procedure proposed by [51]). Subsequent stages recursively optimize one parameter at a time, fixing the other two at their respective latest optimum. Optimizing one variable at a time speeds up convergence but does not ensure achieving the minimum in a single iteration. In general, successive iterations may be needed. In all the examined case studies, however, no iteration beyond the first one results necessary. An additional advantage of the proposed procedure is that the decomposition of the 3D optimization into 1D optimizations logically follows the traditional TMD design practice of first fixing μ, then tuning r and finally adjusting ζ, and offers a clear understanding of the dependence of C on each TMD parameter. As to the more appropriate algorithm to solve the resulting 1D optimizations expressed by Eqs. (22) to (27), any available technique is in principle welcome, and substantially equivalent in the scope of the present paper. It should be emphasized that the proposed iterative procedure, far from generally ensuring convergence to a formal optimum, proves very effective for the specific problem at hand, because of two important circumstances: first, the initial H_∞^f design is very close to the optimum; second, the LCC objective is a regular function of the TMD parameters around the optimum. It also deserves noticing that the proposed LCC design might have been alternatively formulated as a multi-objective (Pareto) optimization, by taking the building lifetime cost and the TMD initial cost as two distinct objective functions rather than summing them up into a single objective. Past studies on TMD LCC optimization have used either the single- [24] or the multi-objective approach [30]. Although the more advanced multi-objective approach generally allows for a more comprehensive understanding of the trade-off among competing objectives, the single-objective formulation, directly providing the non-dominated solution at the minimum total cost, has been here preferred. In fact, the TMD initial cost practically coincides (but from a multiplicative constant) with the TMD mass ratio (i.e. the first design variable), so that the trade-off between the two objectives is substantially expressed by the μ-C curves obtained at the stage 1 of the optimization (see Figure 6 next), which indeed approximate a Pareto front.

Iteration 1 - Stage 1: $$C_{opt}^{1,1} = \min_{\mu} C\left(\mu, r_{opt,H}(\mu), \varsigma_{opt,H}(\mu)\right), \quad \mu \le \mu_{\max} \rightarrow \mu_{opt}^{1,1} \tag{22}$$

Iteration 1 - Stage 2: $$C_{opt}^{1,2} = \min_{r} C\left(\mu_{opt}^{1,1}, r, \varsigma_{opt,H}(\mu_{opt}^{1,1})\right) \rightarrow r_{opt}^{1,2} \tag{23}$$

Iteration 1 - Stage 3: $$C_{opt}^{1,3} = \min_{\varsigma} C\left(\mu_{opt}^{1,1}, r_{opt}^{1,2}, \varsigma\right) \rightarrow \varsigma_{opt}^{1,3} \tag{24}$$

Iteration k - Stage 1: $$C_{opt}^{k,1} = \min_{\mu} C\left(\mu, r_{opt}^{k-1,2}, \varsigma_{opt}^{k-1,3}\right), \quad \mu \le \mu_{\max} \rightarrow \mu_{opt}^{k,1} \tag{25}$$

Iteration k - Stage 2: $$C_{opt}^{k,2} = \min_{r} C\left(\mu_{opt}^{k,1}, r, \varsigma_{opt}^{k-1,3}\right) \rightarrow r_{opt}^{k,2} \quad (26)$$

Iteration k - Stage 3: $$C_{opt}^{k,3} = \min_{\varsigma} C\left(\mu_{opt}^{k,1}, r_{opt}^{k,2}, \varsigma\right) \rightarrow \varsigma_{opt}^{k,3} \quad (27)$$

3 Example: seismic improvement of existing MRF buildings through TMDs

3.1 Premise

In this Section, the methodology detailed in Section 2 is applied to the seismic improvement of three inelastic structural models, representative of existing standard office buildings located in high seismic hazard regions. These are the 3-, 9- and 20-storey steel MRF buildings designed for the Los Angeles (LA) region by Brandow & Johnston Associates within the SAC Phase II Steel Project [43], and later turned into the three benchmark control problems for seismically excited nonlinear buildings [42]. The structures, here called B03, B09 and B20 for brevity, are designed as standard low-, medium- and high-rise office buildings according to UBC 1994, following all code requirements for gravity, wind and seismic design. Although not actually constructed, the buildings represent typical steel MRFs in LA, conceived according to pre-Northridge design practice. In this example, a 50-year lifetime period t and a 2%/year discount rate λ are assumed, resulting in an actualized time period t_a = 31.6 years. To account for the uncertainties inherent in the TMD cost model, the TMD unit cost is alternatively assumed as the lower and upper values proposed in Section 2.3.4, namely c_{UL} = 1250 €/ton and c_{UU} = 2500 €/ton. The maximum admissible TMD mass ratio is set at $\mu_{\max}$ = 10%.

3.2 The structural models

3.2.1 The uncontrolled models

Each benchmark building presents a lateral load-resisting system made of four identical perimeter steel MRFs (two symmetrically distributed MRFs along each horizontal direction), and interior bays with simple framing and composite floors. Because of the in-plan symmetry of the system, a single planar (2D) model, describing one MRF and half the building mass, is used to simulate, according to Eqs. (1) to (4), the structural response of the building, separately along both horizontal directions. The planar models are those implemented by [42] in a set of MATLAB files once available on the web, except that they are here augmented to include P-delta effects and to incorporate the TMD. The models represent ductile steel MRF structures with no strength and stiffness degradation. A concentrated plasticity model is adopted, characterized by a bilinear moment-rotation relationship with 3% strain-hardening. Inertial loads are distributed at the nodes of the respective level based on a lumped mass formulation. Rayleigh damping with a 2% damping ratio in the first two modes is assumed. A detailed description of the three buildings is provided in [43]. Table 4 summarizes their main properties. Figure 2 reports the schematic side view of the three modelled planar frames.

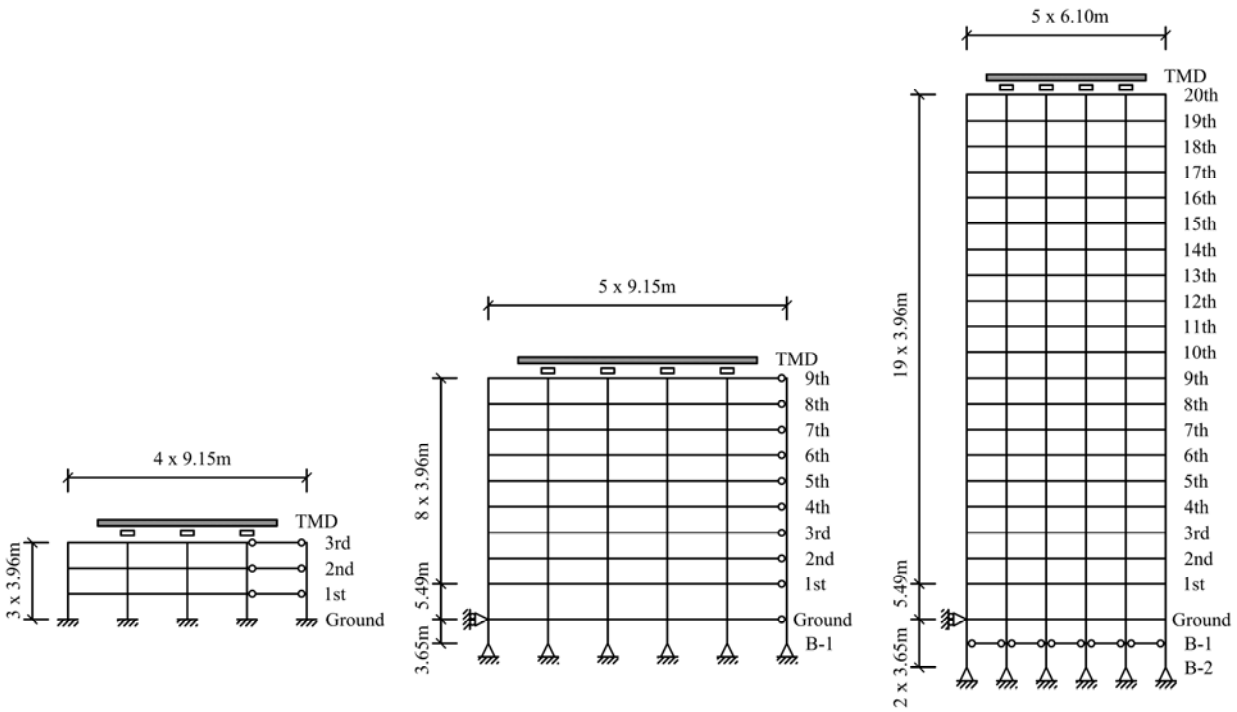
Table 4 Main characteristics of the three benchmark buildings

Building features		B03	B09	B20
Dimensions (m)	Length	36.58 = 4 x 9.15	45.73 = 5 x 9.15	30.48 = 5 x 6.10
	Width	54.87 = 6 x 9.15	45.73 = 5 x 9.15	36.58 = 6 x 6.10
	Height	11.89	37.19	80.77
Seismic masses (kg)	Ground level	-	9.65×10^5	5.32×10^5
	First level	9.57×10^5	10.1×10^5	5.63×10^5
	Top level	10.4×10^5	10.7×10^5	5.84×10^5
	Other levels	9.57×10^5	9.89×10^5	5.52×10^5
Frequencies (Hz) [(i)]	First mode	0.990 (0.977)	0.443 (0.432)	0.261 (0.252)
	Second mode	3.056 (3.031)	1.178 (1.154)	0.753 (0.733)
	Third mode	5.827 (5.792)	2.047 (2.010)	1.299 1.270)

[(i)] In parenthesis: frequencies computed accounting for second-order effects.

3.2.2 The controlled models

For each building, the controlled structural model is obtained by attaching a linear TMD atop, according to Eqs. (1) to (3). Conventionally, the mass ratio μ is assumed as the mass of the TMD divided by the mass of the above-ground building levels, i.e. excluding ground and basement levels. Figure 2 schematizes a possible TMD installation atop the buildings, as an additional floor resting upon appropriate bearings coaxial with the internal columns, so as to uniformly distribute the TMD additional weight upon the inner frames only, without statically affecting the seismically-resisting perimeter MRFs.



(a) B03 (b) B09 (c) B20

Figure 2. Schematics of the three benchmark buildings' elevations.

3.3 The seismic loading

Computing the LCC requires the evaluation of the structural response at N_L levels of increasing intensity. In this work, $N_L = 7$ intensity levels are considered, whose probabilities of exceedance $P_{e/\tau}^{j}$ in the period τ and mean frequencies of exceedance ϕ_e^j are summarized in Table 5. Each intensity level is described by a set of 20 time histories, namely $N_R = 10$ seismic records with 2 orthogonal components each. All sets are defined in accordance with the seismic hazard at the site. Sets 5 to 7 are taken from the SAC steel research project and consist of recorded and simulated ground motions scaled so that their spectral ordinates match, with a least square error fit, the USGS mapped spectral values at 0.3, 1.0 and 2.0 seconds, and an additional predicted value at 4.0 seconds [43]. Sets 1 to 4 are obtained through scaling Set 5 so as to enforce the USGS compatibility at the same four periods. Elastic spectra for sets 5 to 7 are plotted in Figure 3. For each record, the 2D structural model is separately simulated under both horizontal components, in fact providing the full response of the 3D building, by virtue of its in-plan symmetry. From such 3D response, record-EDPs and set-EDPs are subsequently derived as explained in Section 2.3.1.

Table 5 The $N_L = 7$ multiple intensity levels considered in the case-study examples

Set # j	1	2	3	4	5	6	7
$P_{e/\tau}^{j}$ (%)	50	50	50	50	50	10	2
τ (years)	2	5	10	30	50	50	50
ϕ_e^j (n/year)	$3.466 \cdot 10^{-1}$	$1.386 \cdot 10^{-1}$	$6.931 \cdot 10^{-2}$	$2.310 \cdot 10^{-2}$	$1.386 \cdot 10^{-2}$	$2.107 \cdot 10^{-3}$	$4.041 \cdot 10^{-4}$

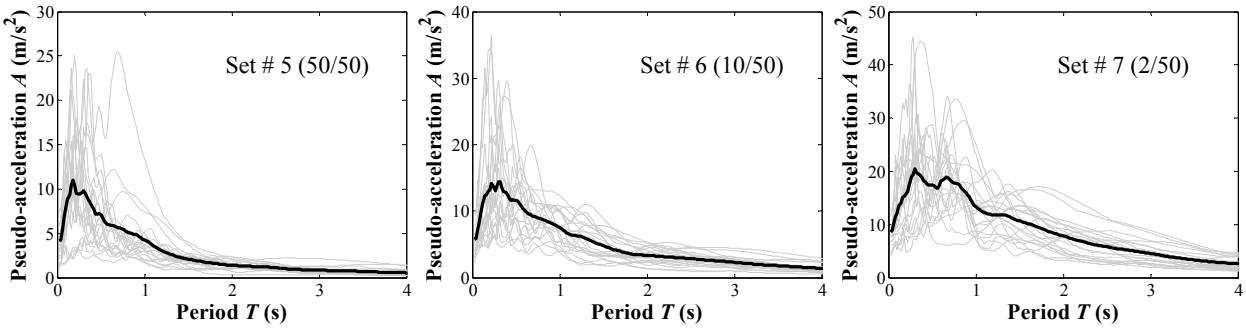


Figure 3. Horizontal pseudo-acceleration 5%-damped elastic spectra for sets 5 to 7. Thin grey lines: individual spectra; thick black lines: mean spectra.

3.4 Conventional TMD design

Before applying, in Section 3.5, the LCC design methodology, the present Section simulates the conventional $H_\infty{}^f$ design of a 5% mass ratio TMD on the 9-storey building, and its subsequent performance evaluation, conducted in either traditional or LCC terms.

3.4.1 Conventional $H_\infty{}^f$ design

In a conventional $H_\infty{}^f$ design, the mass ratio is fixed by the designer, and the optimum frequency and damping ratios are found by minimizing $T_{\theta u}^f$ according to Eq. (18). For building B09, assuming $\mu = 5\%$ leads to $r_{opt,H} = 87.7\%$ and $\zeta_{opt,H} = 19.2\%$, and to an $H_\infty{}^f$ norm $R_{opt,H}$ which is reduced to 15.8% of its uncontrolled value. The corresponding TMD dimensional parameters are $m_T = 4.50 \cdot 10^5$ kg, $\omega_T = 2.37$ rad/s, $k_T = 2.53$ kN/mm and $c_T = 0.410$ kNs/mm.

3.4.2 Traditional performance evaluation

A traditional evaluation of the $H_\infty{}^f$-optimal TMD obtained above is here exemplified, consisting of computing nine performance indices from the mean response of the structure to each of the $N_L = 7$ record sets determined in Section 3.3. These indices are dimensionless quantities obtained, for each set, dividing the controlled mean response by the uncontrolled mean response [42]. Thus, the smaller the index, the better the performance. The indices fall into two main categories: building response and building damage. Denoting by "peak" the largest value in time and by "*h*-max" the largest value along the building height, the first category comprises three peak response measures, namely: the *h*-max peak inter-storey drift ratio (J_1), the *h*-max peak acceleration (J_2) and the peak base shear force (J_3), together with their three root mean square (RMS) analogues, namely: the *h*-max RMS inter-storey drift ratio (J_4), the *h*-max RMS acceleration (J_5) and the RMS base shear force (J_6). The second category comprises three damage measures, namely: the number of damaged members' ends (J_7), the *h*-max dissipated energy factor at members' ends (J_8) and the total dissipated energy factor (J_9).

The said performance indices are reported in Table 6. Expectedly, a progressive performance loss is observed as the intensity level increases, because of structural nonlinearity and TMD mistuning. However, a different trend is observed for each performance index. The large dispersion of the results, apparent in Table 6, points out the need of a unifying and sound LCC-based performance measure.

Table 6 B09: TMD with $\mu = 5\%$ – Performance indices for the $N_L = 7$ intensity levels

Set *j*	J_1	J_2	J_3	J_4	J_5	J_6	J_7	J_8	J_9
1	0.84	0.92	0.72	0.58	0.69	0.50	-	-	-
2	0.84	0.92	0.72	0.58	0.69	0.50	-	-	-
3	0.84	0.92	0.72	0.58	0.69	0.50	0.13	0.02	0.01
4	0.84	0.93	0.74	0.69	0.70	0.50	0.38	0.68	0.72
5	0.85	0.94	0.81	0.72	0.74	0.55	0.49	0.51	0.54
6	0.91	1.02	0.99	0.91	0.81	0.68	0.96	0.73	0.62
7	0.92	1.03	0.98	0.99	0.90	0.82	0.98	0.81	0.84

3.4.3 LCC performance evaluation

The LCC evaluation of the $H_\infty{}^f$-optimal TMD is here conducted according to Section 2.3. In order to show the cost-effectiveness of the TMD, the total controllable lifecycle cost C is computed for the controlled building, decomposed into the building damage cost $C_{DS,S}$, the TMD initial cost $C_{IN,T}$ and the TMD damage cost $C_{DS,T}$, and compared with its uncontrolled counterpart C_{unc}.

The first cost component, i.e. the building damage cost $C_{DS,S}$, is computed according to Eq. (10), where t_a and $C_{DS,S}^{\,i}$ are constant terms independent of the structural response, and ϕ_o^i depends on the building response through the interpolating function $f(\theta)$, according to Eqs. (11) to (14). Figure 4 shows, for example, the function $f(\theta)$ computed for the 8th storey, referred to respectively the uncontrolled case ($\mu = 0\%$) or the controlled case ($\mu = 5\%$). The filled markers represent the "forward step" of the procedure, which involves performing time-history analyses in order to determine the $\phi_e^j - \theta^j$ pairs corresponding to the N_L intensity levels. The white markers represent the "backward step", which implies interpolating between the filled markers in order to extract the $\phi_e^i - \theta^i$ pairs corresponding to the N_D damage states. Similar curves are obtained for the other storeys, as well as for the maximum drift ratio along the building height used for predicting the collapse damage state.

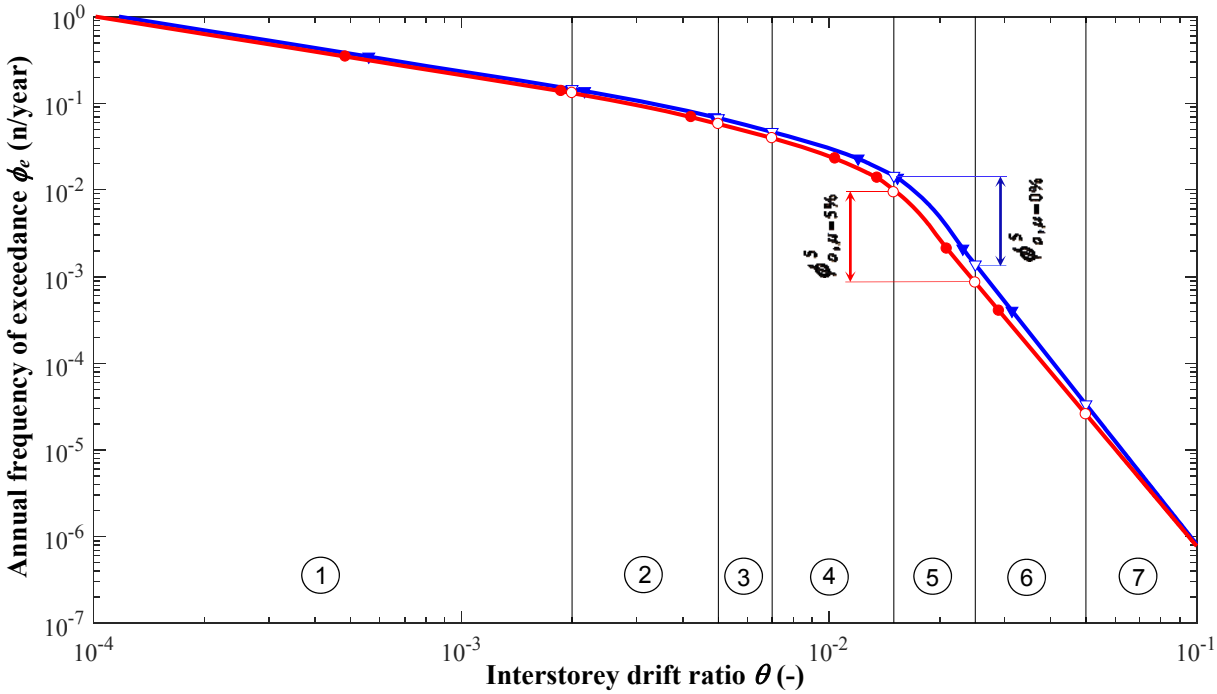


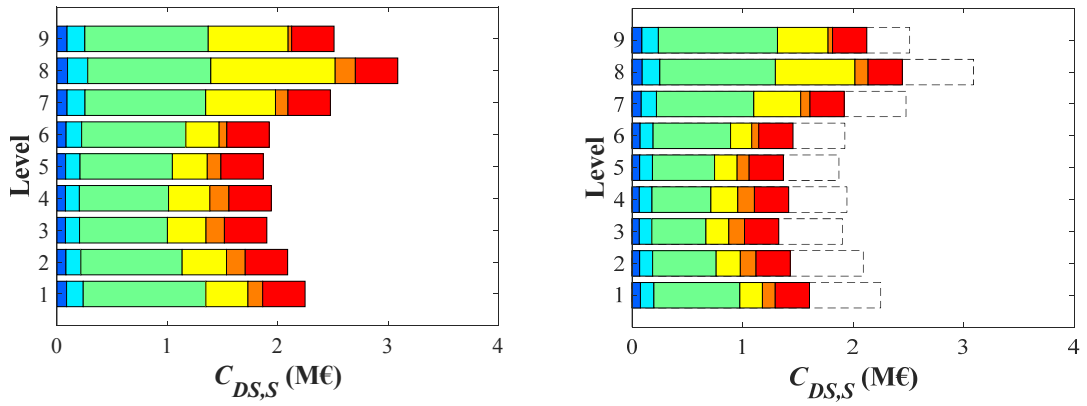
Figure 4. B09: annual frequency of exceedance as a function of the drift ratio, for the 8th storey. Blue curve: $\mu = 0\%$; red curve: $\mu = 5\%$. Filled markers: from analyses; white markers: from fitting.

The resulting $C_{DS,S}$ is reported in Figure 5, for both the uncontrolled (left) and controlled cases (right). Figure 5 decomposes $C_{DS,S}$ into the seven damage states, for each storey level. Since the cost related to the 1st damage state ("1-None") is null, only six damage states are actually represented, from the 2nd one (on the left) to the 7th one (on the right). For the controlled case, a white rectangle with dashed contour is added for comparison, representing the complement to the uncontrolled cost, i.e. the cost saving. Most damage cost is inflicted within the 4th damage state ("4-Moderate") and secondarily within the 5th one ("5-Heavy"), which experience the most expensive combination of occurrence probability and damage severity. These intermediate damage states are also those where TMD cost-effectiveness achieves its best. Within the 4th damage state, the TMD reduces the damage cost to 76% of its uncontrolled value; within the 5th damage state, the reduction is even larger, to 62%. The third most expensive damage state is the 7th one, corresponding to collapse ("7-Destroyed"). Even if the cost reduction for the collapse damage state is less than for the intermediate damage states, it still keeps to an acceptable 81%. By decomposing $C_{DS,S}$ into the seven cost categories instead of the seven damage states, it results that, for both the uncontrolled and controlled cases, the category which contributes the most to $C_{DS,S}$ is damage repair (47%), followed by income (20%), fatalities (16%) and loss of content (15%). The other three categories, i.e. rental, minor and serious injuries, contribute for about 1% each. Summing along the building height, $C_{DS,S}$ turns out to be 20.06 M€ for the uncontrolled structure and 15.09 M€ for the controlled one, resulting in 4.97 M€ in damage cost savings and in a controlled/uncontrolled cost ratio equal to 75%. Repeating the entire procedure using a structural linear model instead of the inelastic one, the controlled/uncontrolled cost ratio would decrease to 70%, indicating that the influence of structural nonlinearity on TMD cost-effectiveness, although not as dramatic as commonly expected, cannot be generally neglected in TMD design.

The second cost component, i.e. the TMD initial cost $C_{IN,T}$, is computed according to Eq. (15). With $\mu = 5\%$, the TMD mass is $m_T = 4.50 \cdot 10^5$ kg. With the lower and upper TMD unit costs identified in Section 2.3.4, $C_{IN,T}$ amounts to, respectively, 0.5625 M€ and 1.125 M€.

The third cost component, i.e. the TMD damage cost $C_{DS,T}$, is computed according to Eq. (16). With $t_a = 31.6$ years and $\phi_o^{N_D} = 2.24 \cdot 10^{-4}$ years^{-1}, $C_{DS,T}$ equals $C_{IN,T}$ times $t_a \phi_o^{N_D} = 7.073 \cdot 10^{-3}$, resulting in, respectively, 3979 € or 7957 €, according as the lower or the upper TMD unit costs are used.

Based on the results above, the total TMD lifecycle cost C_T varies, depending on the TMD unit cost, from 0.57 M€ to 1.13 M€, and is anyway much less than the 4.97 M€ in damage cost savings. The total controllable lifecycle cost C, equal to $C_{unc} = 20.06$ M€ for the uncontrolled building, varies from 15.66 M€ to 16.22 M€ for the controlled building, and the controlled/uncontrolled cost ratio varies accordingly from 78.1% to 80.9%.



(a) $\mu = 0\%$ (uncontrolled) (b) $\mu = 5\%$ (controlled)

Figure 5. B09: building damage cost for the uncontrolled (a) and controlled (b) cases, decomposed among storey levels and damage states. Legend for the damage states, from left to right: 1 (dark blue, not shown); 2 (blue); 3 (azure); 4 (green); 5 (yellow); 6 (orange); 7 (red).

3.5 LCC-optimal TMD design

The LCC-optimal TMD design methodology presented in Section 2.4 is here applied to the three benchmark buildings. Before exposing the results, however, it is useful to illustrate some general features of the objective function C, as they emerge by properly sampling the search space in which the optimization variables μ, r and ζ are defined.

A first, fundamental, result is apparent in Figure 6, where C, decomposed into building damage costs and TMD cost, is plotted versus μ, for the three buildings and the two TMD unit costs.

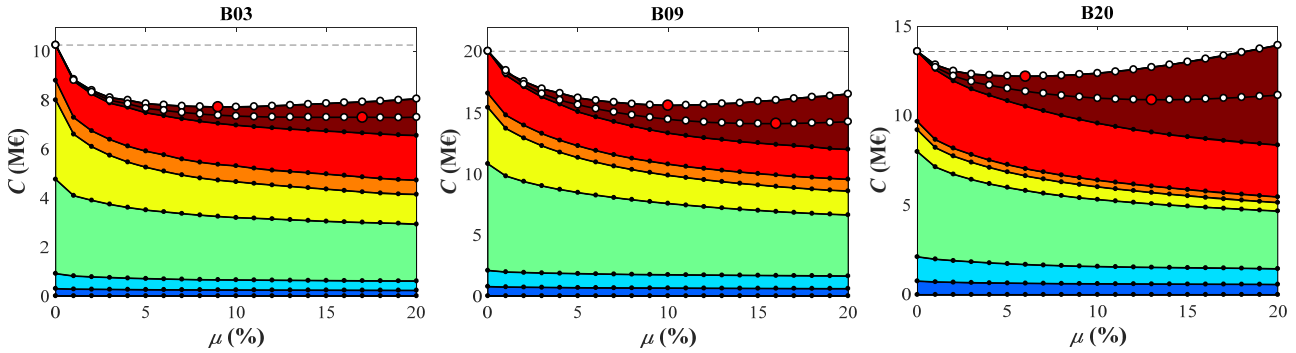


Figure 6. Controllable total cost as a function of the mass ratio, for the three benchmark buildings, decomposed into building damage costs and TMD costs. Legend for damage costs: as in Figure 4. Legend for TMD costs: $c_U = c_{UL}$ (brown under the lower white-dotted curve); $c_U = c_{UU}$ (brown).

For each μ value, r and ζ are kept fixed at their corresponding H_∞[f]-optimal values, i.e. $r_{opt,H}$ and $\zeta_{opt,H}$. The lower and the upper of the two white-dotted curves correspond to, respectively, the lower and the upper TMD unit costs. The red dots identify the minima of the function C, according to the chosen discretization of the horizontal axis. By looking at Figure 6, the following comments can be made:

1) For $\mu = 0$, $C = C_{unc}$ is 10.28 M€, 20.06 M€ and 13.60 M€, respectively for buildings B03, B09 and B20. Divided by the total in-plan area of the 3, 9 and 20 above-ground storeys, these costs result in, respectively, 1707 €/m^2, 1066 €/m^2, and 609.4 €/m^2. The differences among these latter values reflect the differences among the peak inter-storey drift ratios θ obtained from the analyses, which decrease from B03 to B20. This indicates that, from an economic perspective, B03 is the seismically more vulnerable of the three buildings, followed by B09 and then by B20.
2) $C_{DS,S}$, represented for each building by the curve interposed between the red and the brown fields, is a monotonically decreasing convex function of μ. This trend indicates that enlarging the TMD always reduces the building damage cost, but with a progressively lesser marginal gain. For μ equal to 5%, 10% and 20%, $C_{DS,S}$ respectively equals: 73.0%, 68.0% and 63.9% for B03; 75.2%, 66.5% and 59.8% for B09; 79.7%, 70.5% and 61.5% for B20. The monotonic cost decrease is observed in all damage states for all the buildings, except in the collapse damage state for B03, whose cost increases with μ because of the inefficacy of the TMD to reduce the drift ratios at the highest intensity level. The damage state

contributing the most to $C_{DS,S}$ is always the 4th damage state ("4-Moderate"), followed, for B03 and B09, by the 5th one ("5-Heavy") and then by the 7th one ("7-Destroyed"), and for B20 directly by the 7th one, which is a prominent cost component.

3) C_T increases almost linearly with μ, according to Eq. (17). The percentage impact of C_T on C differs among the three buildings as a result of their different seismic vulnerability, and for each building strongly depends on the assumed TMD unit cost.

4) If $c_U = c_{UL}$, C is almost flat for μ around 10÷20%, with optimal μ values located at μ = 17%, 16% and 13%, respectively for B03, B09 and B20. If $c_U = c_{UU}$, large mass ratios become less competitive, particularly for B20. Optimal μ values are in this case around 5÷10%, namely at μ = 9%, 10% and 6%, respectively for B03, B09 and B20. This sensitivity of the optimal μ to the value assumed for c_U points out the importance of relying on accurate TMD cost models.

Other interesting properties of the search space can be appreciated in Figures 7 and 8. Figure 7 shows, for each building, different sections of the search space, corresponding to four possible values of μ (0%, 2%, 5% and 10%, the former coinciding with the uncontrolled case), and obtained by fixing $\zeta = \zeta_{opt,H}$ while varying r around $r_{opt,H}$. Figure 8 is the damping analogue of Figure 7, in which r is fixed and ζ is varied. In both figures, the red dots identify the minima of the function C. Remarkably, Figures 7 and 8 show that the H_∞^f-optimal frequency and damping ratios, $r_{opt,H}$ and $\zeta_{opt,H}$, are close to be LCC-optimal. Even more importantly, they show that C is scarcely sensitive to frequency and damping changes, i.e. that the TMD LCC performance is robust to variations in the TMD parameters.

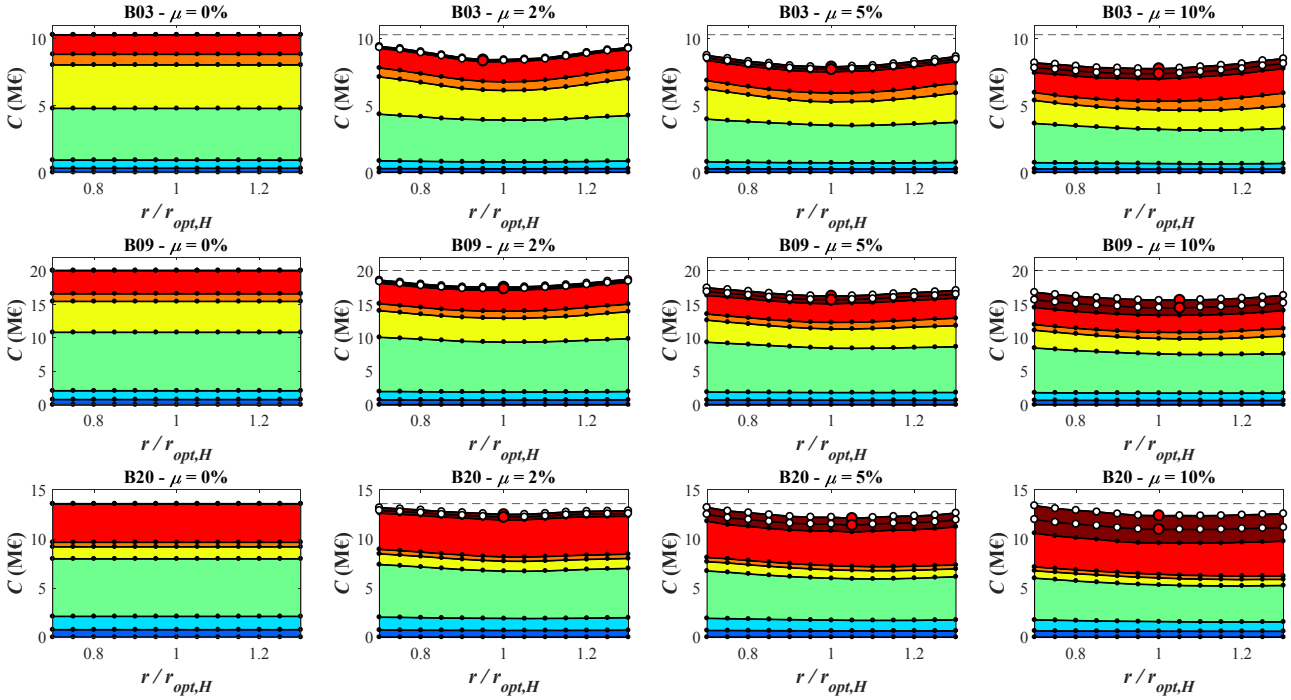


Figure 7. Controllable total cost as a function of the normalized frequency ratio $r/r_{opt,H}$, for the three benchmark buildings and for four possible mass ratios (0%, 2%, 5% and 10%), decomposed into building damage state costs and TMD costs. In all cases, $\zeta = \zeta_{opt,H}$. Legends as in Figure 6.

With such an insight into the structure of the search space, the LCC-optimal design procedure can be run, independently for each building and for the two assumed TMD unit costs. Without loss of generality, optimization is here conducted on a discretized search domain, with a discretization rate equal to 1% for μ and r and to 5% for ζ. Based on the discussion above, this discretization is believed to provide a reasonably close approximation of the exact optimum. Considering for example the B09 building and the larger TMD unit cost, the procedure is detailed as follows:

Iteration 1 - Stage 1: By varying μ, the optimization problem in Eqs. (22) and (23) is solved (see again Figure 6), resulting in $\mu_{opt}^{1,1} = 10\%$ (compatibly with $\mu_{\max} = 10\%$). Correspondingly, the H_∞^f-optimal parameters are $r_{opt,H} = 0.781$ and $\zeta_{opt,H} = 0.267$, and $C_{opt}^{1,1} = 15.61$ M€, i.e. the 77.81% of C_{unc}.

Iteration 1 - Stage 2: By varying r while keeping fixed μ and ζ, the optimization problem in Eqs. (24) and (25) is solved, providing $r_{opt}^{1,2} = 1.03 \cdot r_{opt,H} = 0.804$ (Figure 9a). The corresponding cost is $C_{opt}^{1,2} = 15.60$ M€, i.e. the 77.76% of C_{unc}.

Iteration 1 - Stage 3: By varying ζ while keeping fixed μ and r, the optimization problem in Eqs. (26) and (27) is solved, providing $\zeta_{opt}^{1,3} = 0.90 \cdot \zeta_{opt,H} = 0.240$ (Figure 9b). The corresponding cost is $C_{opt}^{1,3} = 15.57$ M€, i.e. the 77.61% of C_{unc}.

Iteration 2 - Stages 1 to 3: Repeating Stages 1 to 3 starting from the solution obtained at the end of Iteration 1 does not further change that solution, which is concluded to be the LCC-optimum.

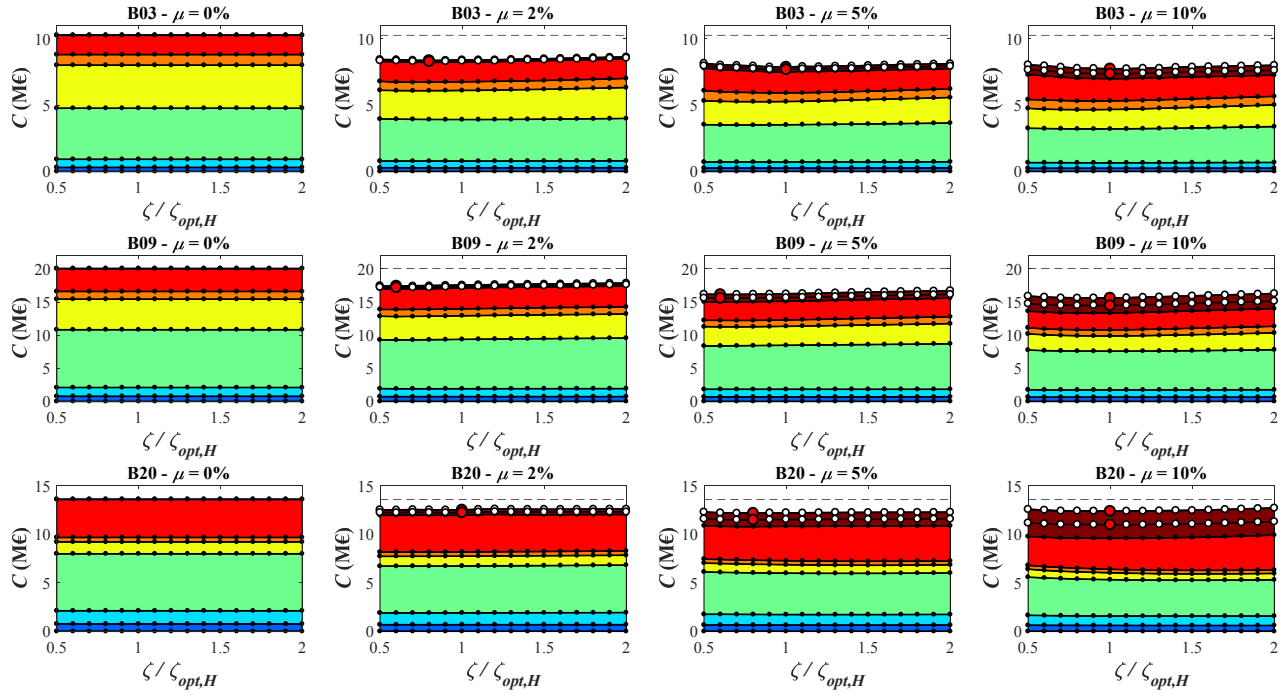


Figure 8. Controllable total cost as a function of the normalized damping ratio $\zeta/\zeta_{opt,H}$, for the three benchmark buildings and for four possible mass ratios (0%, 2%, 5% and 10%), decomposed into building damage state costs and TMD costs. In all cases, $r = r_{opt,H}$. Legends as in Figures 6 and 7.

Repeated for the three buildings and the two TMD unit costs, the procedure is summarized in Tables 7 to 12. Each row corresponds to a different Stage of Iteration 1. Iteration 2 is not shown, because in all cases it would confirm the solution found at the end of Iteration 1. In columns 3 to 5, the TMD parameters are reported as they evolve towards optimality; in columns 6 to 8, $C_{DS,S}$, C_T and C are reported, normalized to C_{unc}. In Tables 7, 9 and 11, an initial row is added providing the unconstrained optimal solution obtained at Iteration 1 - Stage 1 prior to imposing the condition $\mu_{max} = 10\%$.

Table 7 LCC optimization procedure for building B03 under the assumption of the lower TMD unit cost

Iteration	Stage	μ_{opt}	$r_{opt}/r_{opt,H}$ [a]	$\zeta_{opt}/\zeta_{opt,H}$ [a]	$C_{DS,S}/C_{unc}$ [b]	C_T/C_{unc} [b]	C/C_{unc} [b]
1	1	**0.17** > 0.10	1.00	1.00	0.649	0.062	0.711
1	1	**0.10**	1.00	1.00	0.680	0.037	0.717
1	2	0.10	**1.00**	1.00	0.680	0.037	0.717
1	3	0.10	1.00	**1.00**	0.680	0.037	0.717

Note [a]: $r_{opt,H} = 0.803$ and $\zeta_{opt,H} = 0.243$ for $\mu = 10\%$. Note [b]: $C_{unc} = 10.279$ M€.

Table 8 LCC optimization procedure for building B03 under the assumption of the higher TMD unit cost

Iteration	Stage	μ_{opt}	$r_{opt}/r_{opt,H}$ [a]	$\zeta_{opt}/\zeta_{opt,H}$ [a]	$C_{DS,S}/C_{unc}$ [b]	C_T/C_{unc} [b]	C/C_{unc} [b]
1	1	**0.09**	1.00	1.00	0.687	0.066	0.753
1	2	0.09	**1.03**	1.00	0.685	0.066	0.751
1	3	0.09	1.03	**1.00**	0.685	0.066	0.751

Note [a]: $r_{opt,H} = 0.817$ and $\zeta_{opt,H} = 0.232$ for $\mu = 9\%$. Note [b]: $C_{unc} = 10.279$ M€.

Table 9 LCC optimization procedure for building B09 under the assumption of the lower TMD unit cost

Iteration	Stage	μ_{opt}	$r_{opt}/r_{opt,H}$ [(a)]	$\zeta_{opt}/\zeta_{opt,H}$ [(a)]	$C_{DS,S}/C_{unc}$ [(b)]	C_T/C_{unc} [(b)]	C/C_{unc} [(b)]
1	1	**0.16** > 0.10	1.00	1.00	0.618	0.091	0.709
1	1	**0.10**	1.00	1.00	0.665	0.057	0.721
1	2	0.10	**1.03**	1.00	0.664	0.057	0.721
1	3	0.10	1.03	**0.90**	0.663	0.057	0.719

Note [(a)]: $r_{opt,H} = 0.781$ and $\zeta_{opt,H} = 0.267$ for $\mu = 10\%$. Note [(b)]: $C_{unc} = 20.058$ M€.

Table 10 LCC optimization procedure for building B09 under the assumption of the higher TMD unit cost

Iteration	Stage	μ_{opt}	$r_{opt}/r_{opt,H}$ [(a)]	$\zeta_{opt}/\zeta_{opt,H}$ [(a)]	$C_{DS,S}/C_{unc}$ [(b)]	C_T/C_{unc} [(b)]	C/C_{unc} [(b)]
1	1	**0.10**	1.00	1.00	0.665	0.113	0.778
1	2	0.10	**1.03**	1.00	0.664	0.113	0.778
1	3	0.10	1.03	**0.90**	0.663	0.113	0.776

Note [(a)]: $r_{opt,H} = 0.781$ and $\zeta_{opt,H} = 0.267$ for $\mu = 10\%$. Note [(b)]: $C_{unc} = 20.058$ M€.

Table 11 LCC optimization procedure for building B20 under the assumption of the lower TMD unit cost

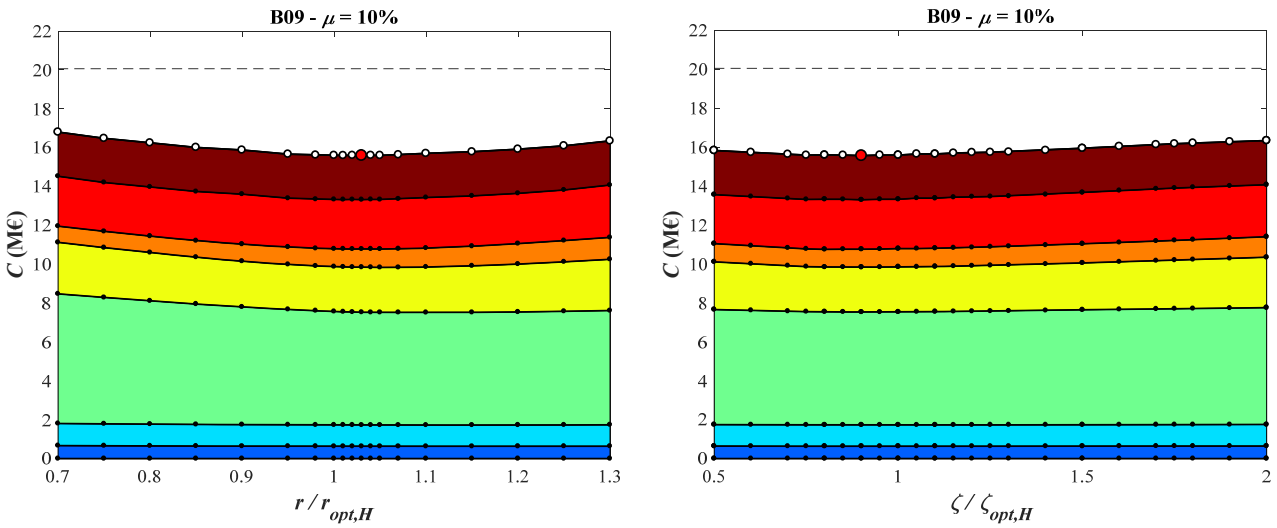
Iteration	Stage	μ_{opt}	$r_{opt}/r_{opt,H}$ [(a)]	$\zeta_{opt}/\zeta_{opt,H}$ [(a)]	$C_{DS,S}/C_{unc}$ [(b)]	C_T/C_{unc} [(b)]	C/C_{unc} [(b)]
1	1	**0.13** > 0.10	1.00	1.00	0.668	0.134	0.801
1	1	**0.10**	1.00	1.00	0.705	0.103	0.807
1	2	0.10	**1.08**	1.00	0.702	0.103	0.805
1	3	0.10	1.08	**0.80**	0.700	0.103	0.802

Note [(a)]: $r_{opt,H} = 0.787$ and $\zeta_{opt,H} = 0.265$ for $\mu = 10\%$. Note [(b)]: $C_{unc} = 13.890$ M€.

Table 12 LCC optimization procedure for building B20 under the assumption of the higher TMD unit cost

Iteration	Stage	μ_{opt}	$r_{opt}/r_{opt,H}$ [(a)]	$\zeta_{opt}/\zeta_{opt,H}$ [(a)]	$C_{DS,S}/C_{unc}$ [(b)]	C_T/C_{unc} [(b)]	C/C_{unc} [(b)]
1	1	**0.06**	1.00	1.00	0.774	0.123	0.897
1	2	0.06	**1.06**	1.00	0.767	0.123	0.891
1	3	0.06	1.06	**1.00**	0.767	0.123	0.891

Note [(a)]: $r_{opt,H} = 0.855$ and $\zeta_{opt,H} = 0.211$ for $\mu = 6\%$. Note [(b)]: $C_{unc} = 13.890$ M€.



(a) Iteration 1 – Stage 2 (b) Iteration 1 – Stage 3

Figure 9. Controllable total cost as a function of: (a) $r/r_{opt,H}$ (Iter. 1 - Stage 2); (b) $\zeta/\zeta_{opt,H}$ (Iter. 1 - Stage 3), for B09 and $\mu = 10\%$. Legend for damage state costs: as in Fig. 4. Legend for TMD costs: $c_U = c_{UU}$ (brown).

Based on Tables 7 to 12, the following considerations can be formulated:

1) The procedure rapidly converges, with no need of a second iteration. This is partly due to the search being conducted on a discretized search domain, but mostly to the plain structure of the search domain and the adequacy of the H_∞^f-optimum to closely approximate the LCC-optimum.
2) The distance of the LCC-optimum from the H_∞^f-optimum is variable in terms of r (0÷8%) and ζ (0÷20%) but is always small in terms of C (0÷0.75%, and less than 0.3% for B03 and B09). This confirms the

robustness of the optimal solution to r and ζ, and corroborates the validity of the H_∞^f-design to closely approximate the LCC-optimum.

3) The TMD unit cost is a crucial parameter in the optimization process: halving c_U nearly doubles μ_{opt}. Accurate TMD cost models are therefore fundamental. In the examined case studies, assuming $c_U = c_{UL}$ leads to very large values of μ_{opt} (between 13% and 17%), at least until the $\mu_{max} = 10\%$ constraint is enforced. This result confirms and expands the conclusions of recent researches by the author, advocating the use of very large mass ratios to achieve a satisfactory TMD seismic performance on linear structures [8]. Even the assumption of $c_U = c_{UU}$ leads, anyway, to uncommonly large μ_{opt} values (between 6% and 10%). For $c_U = c_{UL}$, the bound imposed on μ_{max} eventually implies $\mu_{opt} = 10\%$ for every building.
4) Considering, first, the lower TMD unit cost, the obtained large optimal mass ratio ($\mu_{opt} = 10\%$) entails large and similar reductions of the normalized building damage cost $C_{DS,S} / C_{unc}$ for the three buildings, equal to 68%, 66% and 70% respectively. The normalized TMD total cost C_T / C_{unc} results, instead, quite different among the three buildings because of their different seismic vulnerability, and equal to respectively 3.7%, 5.7% and 10.3%. As a result, the corresponding normalized total cost C / C_{unc} is similar for buildings B03 and B09 (72%) and higher for building B20 (80%). Remarkably, the TMD cost equals, for the three buildings, only 11%, 17% and 34% of the achieved reduction in damage costs.
5) Considering, then, the upper TMD unit cost, the obtained optimal mass ratios are different for the three buildings, larger for B03 ($\mu_{opt} = 9\%$) and B09 ($\mu_{opt} = 10\%$), and smaller for B20 ($\mu_{opt} = 6\%$). As a result, larger reductions in $C_{DS,S} / C_{unc}$ are obtained for B03 (68%) and B09 (66%), and a lesser reduction is obtained for B20 (77%). With respect to assuming the lower unit cost, C_T / C_{unc} obviously increases, respectively to 6.6%, 11.3% and 12.3%, and C / C_{unc} increases too, moderately for B03 (75%) and B09 (78%) and drastically for B20 (90%). The TMD cost now equals, for the three buildings, 21%, 34% and 55% of the achieved reduction in damage costs.

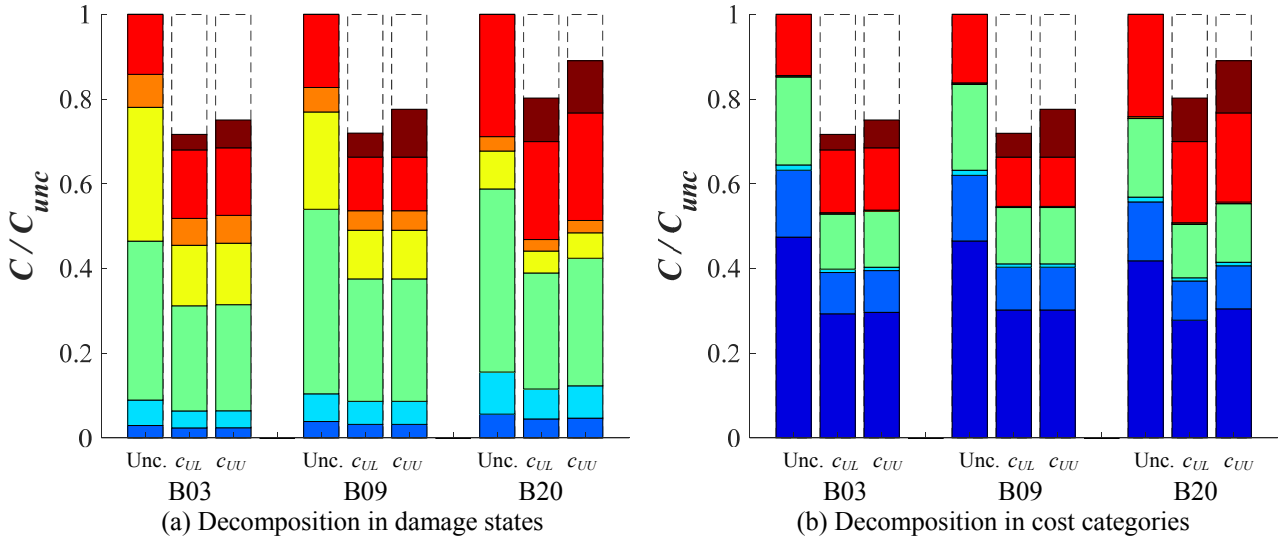
Not reported in Tables 7 to 12, the TMD stroke demand computed for the optimized TMD under the most severe of the 7 seismic levels results to be on average 0.312 m, 0.850 m and 1.051 m for, respectively, buildings B03, B09 and B20 (where, for brevity, the geometric mean has been taken of the results derived from respectively the lower and upper TMD unit cost assumptions). These values, naturally increasing with the fundamental structural period, are in line with expectations and reasonably acceptable from a practical perspective.

The optimal solutions outlined above are compared with their uncontrolled counterparts in Figure 10. $C_{DS,S}$ is alternatively decomposed into damage states (Figure 10a) and cost categories (Figure 10b). The brown rectangles represent the TMD cost, the white rectangles with dashed contours represent the total cost savings. For each building, the left column refers to the uncontrolled configuration, the central and the right columns refer to the two controlled configurations, respectively based on c_{UL} and c_{UU}. The TMD cost-effectiveness is apparent in all cases, higher for B03 and B09 and for c_{UL}, lower but still significant for B20 and/or c_{UU}. Among the damage states, the one which, in percentage, benefits the more from the intervention is the 5th ("5-Heavy"), followed by the 4th ("4-Moderate") and then by the 3rd ("3-Light"). All damage state costs are reduced by the intervention, with the only exception of the collapse damage state cost ("7-Destroyed"), which increases by 13% for building B03 (while decreasing by 27% for B09 and by 16% for B20). Among the cost categories, those which, in percentage, benefit the more are the first four ones (damage repair, loss of content, rental and income). The last category, human fatality, is unfortunately the one which benefits the less, with a cost decreasing by 28% for B09 and by 17% for B20, and indeed increasing by 2% for B03. These results prove that the TMD performance may be poor or even detrimental for inelastic structures under extreme seismic intensities but that this is not a general rule, and that the large economic benefits achieved in mitigating the less severe damage states still ensure the overall cost-effectiveness of this control system, making a TMD installation a profitable investment.

Two final considerations can be done, based on the additional results reported in Figure 11.

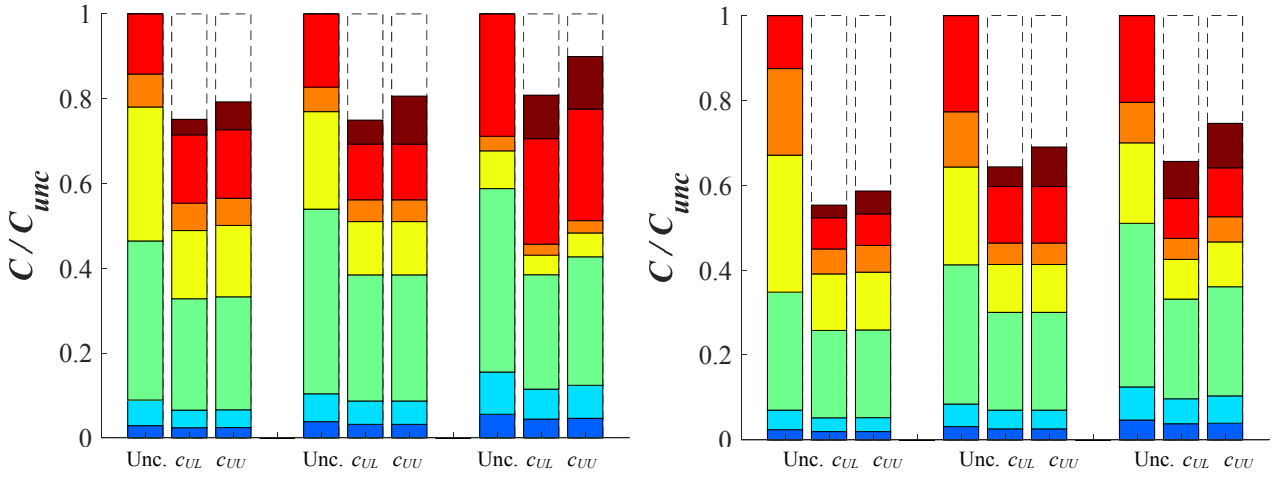
Figure 11a is identical to Figure 10a, except that it is obtained assuming for the TMD a damping ratio which is twice its optimal value. As a result, the building damage cost $C_{DS,S}$ increases on average by 6.1%, 4.5% and 1.0%, respectively for buildings B03, B09 and B20. At the same time, the TMD stroke demand computed under the most severe seismic level respectively decreases by 34.2%, 33.1% and 32.8% for the three buildings (i.e. to 0.205 m for B03, 0.569 m for B09 and 0.706 m for B20). These results indicate that increasing the amount (and therefore the cost) of damping in a TMD may indeed reduce the cost due to accommodating large stroke demands, with very little influence on the TMD LCC performance. In order to rigorously incorporate

these issues in a LCC TMD optimization, however, an improved TMD cost model would be obviously required.



(a) Decomposition in damage states (b) Decomposition in cost categories

Figure 10. Optimal C for the three buildings and the two TMD unit costs, decomposed into TMD cost and the costs of either damage states (a) or cost categories (b). For each building: uncontrolled case (left); controlled with c_{UL} (middle); controlled with c_{UU} (right). Damage states: as in Figure 4. Cost categories: C^i_{dam} (dark blue); C^i_{con} (blue); C^i_{ren} (azure); C^i_{inc} (green); $C^i_{inj,m}$ (yellow); C^i_{inj} (orange); C^i_{fat} (red). TMD: brown rectangle.



(a) Doubling the TMD damping ratio (b) Assuming a linear model

Figure 11. Two variants of Figure 10a: (a) as in Figure 10a except that the TMD damping ratio is doubled; (b) as in Figure 10a except that the structural model is assumed linear.

Figure 11b is the analogue of Figure 10a, except that it is obtained assuming for the building structure a linear model instead of the (correct) nonlinear one. By comparing the two figures, it results that, for the examined case studies, the incorrect linear model largely overestimates TMD advantages. In fact, the values of $C_{DS,S}/C_{unc}$ obtained with the linear model equal 77.3%, 90.1% and 82.4% of the corresponding values obtained with the nonlinear model, for respectively B03, B09 and B20. The overestimation is mostly concentrated into damage states 6 and 7 (corresponding to the largest inelastic excursions), where the (unrealistic) linear analysis depicts an excellent TMD performance whilst the (rigorous) nonlinear evaluation testifies the substantial inefficacy of the absorber. On the one hand, these results prove that a "linearized" LCC analysis cannot be generally used to portrait the lifetime performance of TMDs on inelastic structures, at least in high seismic hazard regions, where significant damage costs may be inflicted to the structure within its nonlinear response range. Of course, the extent of such overestimation is problem dependent, and likely to become small or negligible for low-to-moderate seismic hazards, when inelasticity slightly affects LCC. Further insight into this point will come from extending the present study to a greater variety of structures and seismic intensities, which is left for future work. On the other hand, the same results help explaining why the optimal frequency and damping ratios

obtained through the nonlinear LCC design are not far from those provided by the conventional linear H_∞^f approach: for moderate ground motions the linear design is intrinsically optimal, while for large seismic intensities the TMD is of little use, independently of the adopted design. Indeed, the main advantage of a nonlinear TMD LCC design appears to be not so much the fine tuning of r and ζ, as in standard optimization strategies, but the correct quantification of costs and benefits, which eventually allows for the optimal choice of μ. In this regard, a linear LCC design, since overestimating the cost savings brought by TMD installation, would lead to a biased optimization, i.e. to a mass ratio larger than optimal. The exact quantification of such bias is left for future study.

4 Conclusions

In this paper, an LCC optimization of TMDs for the seismic improvement of building structures is proposed which can account for their inelastic response, and is applied to the simulated upgrade of three benchmark structures, taken as representative of standard steel MRF office buildings located in highly seismic regions. Main conclusions of this study can be summarized as follows:

1) For ordinary buildings in highly seismic regions, exhibiting large inelastic excursions under severe seismic intensities, both conventional performance criteria and linearized LCC approaches may be inadequate to portrait the TMD advantages: the former because amplitude-dependent and unable to concisely measure the TMD cost-effectiveness; the latter because inaccurate in approximating the actual inelastic response. In these cases, a fully nonlinear LCC evaluation framework is required to reliably portrait costs and benefits of the TMD.
2) In the examined examples, the proposed iterative LCC design, consisting of a series of 1D optimizations starting from a preliminary H_∞^f design, proves simple and effective. It rapidly converges to a near-optimal solution if an appropriate discretization of the TMD parameters is adopted, and offers a clear understanding of the search space.
3) Stage 1 at Iteration 1 is the decisive step of the procedure. Fixing the TMD frequency and damping ratios, r and ζ, to their H_∞^f-optimal values, makes the optimization problem a 1D search for the nearly-optimal mass ratio μ. In the considered examples, this value indeed coincides with the LCC-optimal μ, and the corresponding LCC gets very close to the exact minimum. Therefore, Stage 1 at Iteration 1 proves an expedient tool for an approximate LCC design. Its graphical representation offers a deep insight into the TMD cost-benefit trade-off.
4) Subsequent stages further improve r and ζ with respect to their pre-assigned H_∞^f-optimal values. The improvement is small in terms of r and ζ, and negligible in terms of the LCC. This shows the robustness of the solution to changes in r and ζ, and corroborates the validity of the H_∞^f-design as a preliminary design tool. Because a conventional design (like the H_∞^f) performs well even for nonlinear structures, the true merit of a nonlinear LCC design is not in the fine tuning of r and ζ, as in standard optimization strategies, but in the correct quantification of costs and benefits of the TMD, eventually allowing for the optimal μ.
5) The optimum proves sensitive to the TMD unit cost, instead. In the lack of more accurate TMD cost models, the adopted mass-proportional cost relation, with lower and upper unit costs, sounds a reasonable compromise among the few formulations available in the literature, which certainly requires further confirmation.
6) With such a TMD cost model, the optimal μ ranges, depending on the building, from 13% to 17% if the lower unit cost is assumed, and from 6% to 10% if the upper unit cost is taken. This result agrees with recent studies on the efficacy of TMDs on linear structures, advocating the use of large mass ratios to achieve a satisfactory seismic performance.
7) LCC-optimal TMDs considerably reduce the total LCC of the building-damper system, to an extent which depends on the building vulnerability and on the TMD unit cost. For the three examined buildings, the total LCC reduces to 72%, 72% and 80% of its uncontrolled value if the lower unit cost is assumed, and to the 75%, 78% and 90% if the upper unit cost is taken. In all cases, the TMD-based seismic improvement proves a profitable investment.

References

[1] Spencer BF Jr., Nagarajaiah S (2003) State of the Art of Structural Control. J Struct Eng 129(7):845-856
[2] Warburton GB (1982) Optimum absorber parameters for various combinations of response and excitation parameters. Earthq Eng Struct Dyn 10:381-401

[3] Wirsching PH, Campbell GW (1974) Minimal structural response under random excitation using vibration absorber. Earthq Eng Struct Dyn 2:303-312
[4] Jagadish KS, Prasad BKR, Rao PV (1979) The inelastic vibration absorber subjected to earthquake ground motions. Earthq Eng Struct Dyn 7:317-326
[5] Villaverde R, Koyama LA (1993) Damped resonant appendages to increase inherent damping in buildings. Earthq Eng Struct Dyn 22:491-507
[6] Sadek F, Mohraz B, Taylor AW, Chung RM (1997) A method of estimating the parameters of tuned mass dampers for seismic applications. Earthq Eng Struct Dyn 26:617-635
[7] Hoang N, Fujino Y, Warnitchai P (2008) Optimal tuned mass damper for seismic applications and practical design formulas. Eng Struct 30(3):707-715
[8] Matta E (2011) Performance of tuned mass dampers against near-field earthquakes. Struct Eng Mech 39(5):621-642
[9] Matta E (2013) Effectiveness of tuned mass dampers against ground motion pulses. J Struct Eng 139(2):188-198
[10] Kaynia AM, Veneziano D, Biggs JM (1981) Seismic effectiveness of tuned mass dampers. J Struct Eng 107(8):1465-1484
[11] Sladek JR, Klingner RE (1983) Effect of tuned mass dampers on seismic response. J Struct Eng 109(8):2004-2009
[12] Chowdhury AH, Iwuchukwu MD, Garske JJ (1985) Past and future of seismic effectiveness of tuned mass dampers, in: Proceedings of the 2nd Int. Symp. on Struct. Control, Ontario, Canada, 105-127
[13] Ruiz SE, Esteva L (1997) About the effectiveness of tuned mass dampers on nonlinear systems subjected to earthquakes, In: Manolis GD, Beskos DE, Brebbia CA (eds) WIT Press. Earthquake resistant engineering structures. Advances in earthquake engineering 2:311-320
[14] Soto-Brito R, Ruiz SE (1999) Influence of ground motion intensity on the effectiveness of tuned mass dampers. Earthq Eng Struct Dyn 28:1255-1271
[15] Lukkunaprasit P, Wanitkorkul A (2001) Inelastic buildings with tuned mass dampers under moderate ground motions from distant earthquakes. Earthq Eng Struct Dyn 30:537-551
[16] Pinkaew T, Lukkunaprasit P, Chatupote P (2003) Seismic effectiveness of tuned mass dampers for damage reduction of structures. Eng Struct 25:39-46
[17] Wong KKF (2008) Seismic energy dissipation of inelastic structures with tuned mass dampers. J Eng Mech 134(2):163-172
[18] Wong KKF, Harris JL (2012) Seismic damage and fragility analysis of structures with tuned mass dampers based on plastic energy. Struct Des Tall Spec Build 21:296-310
[19] Zhang Z, Balendra T (2013) Passive control of bilinear hysteretic structures by tuned mass damper for narrow band seismic motions. Eng Struct **54**:103-111
[20] Beck JL, Porter KA, Shaikhutdinov RV (2003) Simplified estimation of seismic life-cycle costs, In: Frangopol DM, Bruhwiler E, Faber MH, Adey B (eds) Life-cycle performance of deteriorating structures: assessment, design, and management 229-236
[21] Sanchez-Silva M, Rackwitz R (2004) Socioeconomic implications of life quality index in design of optimum structures to withstand earthquakes. J Struct Eng 130(6):969-977
[22] Goulet CA, Haselton CB, Mitrani-Reiser J, Beck JL, Deierlein GG, Porter KA, Stewart JP (2007) Evaluation of the seismic performance of a code-conforming reinforced-concrete frame building - from seismic hazard to collapse safety and economic losses, Earthq Eng Struct Dyn 36:1973-1997
[23] Kappos AJ, Dimitrakopoulos EG (2008) Feasibility of pre-earthquake strengthening of buildings based on cost-benefit and life-cycle cost analysis, with the aid of fragility curves. Nat Hazards 45(1):33-54
[24] Taflanidis AA, Beck JL (2009) Life-cycle cost optimal design of passive dissipative devices. Struct Saf 31:508-522
[25] Shin H, Singh MP (2014) Minimum failure cost-based energy dissipation system designs for buildings in three seismic regions – Part I: Elements of failure cost analysis. Eng Struct 74:266-274
[26] Hahm D, Ok S-Y, Park W, Koh H-M, Park K-S (2013) Cost-effectiveness evaluation of an MR damper system based on a life-cycle cost concept. KSCE J Civ Eng 17(1):145-154
[27] Huang MF, Tse KT, Chan CM, Lou WJ (2011) Integrated structural optimization and vibration control for improving wind-induced dynamic performance of tall buildings. Int J Struct Stab Dyn 11(6):1139-1161
[28] Wang D, Tse TKT, Zhou Y, Li Q (2015) Structural performance and cost analysis of wind-induced vibration control schemes for a real super-tall building. Struct Infrastruct Eng 11(8): 990-1011

[29] Ruiz R, Taflanidis AA, Lopez-Garcia D, Vetter CR (2016) Life-cycle based design of mass dampers for the Chilean region and its application for the evaluation of the effectiveness of tuned liquid dampers with floating roof. Bull Earthq Eng 14:943-970.
[30] Greco R, Marano GC, Fiore A (2016) Performance-cost optimization of tuned mass damper under low-moderate seismic actions. Struct Des Tall Spec Build 25:1103-1122
[31] Taflanidis AA, Angelides DC, Scruggs JT (2009) Simulation-based robust design of mass dampers for response mitigation of tension leg platforms. Eng Struct 31:847-857
[32] Lee CS, Goda K, Hong HP (2012) Effectiveness of using tuned-mass dampers in reducing seismic risk. Struct Infrastruct Eng 8(2):141-156
[33] Matta E (2015) Seismic effectiveness of tuned mass dampers in a life-cycle cost perspective. Earthq Struct 9(1):73-91
[34] Kong JS, Frangopol DM (2003) Life-cycle reliability-based maintenance cost optimization of deteriorating structures with emphasis on bridges. J Struct Eng 129(6):818-28
[35] Ang H-SA, Lee J-C (2001) Cost optimal design of R/C buildings. Reliab Eng System Safe 73:233-8
[36] Liu M, Burns SA, Wen YK (2003) Optimal seismic design of steel frame buildings based on life cycle cost considerations. Earthq Eng Struct Dyn 32:1313-32
[37] Fragiadakis M, Lagaros ND, Papadrakakis M (2006) Performance-based multiobjective optimum design of steel structures considering life-cycle cost. Struct Multidiscip Optim 32:1-11
[38] Wen YK, Kang YJ (2001) Minimum building life-cycle cost design criteria. II: Applications. J Struct Eng 127(3):338-346
[39] Lagaros ND, Fotis AD, Krikos SA (2006) Assessment of seismic design procedures based on the total cost. Earthq Eng Struct Dyn 35:1381-1401
[40] Fragiadakis M, Lagaros ND (2011) An overview to structural seismic design optimisation frameworks. Comput and Struct 89:1155-1165
[41] Mitropoulou CC, Lagaros ND, Papadrakakis M (2011) Life-cycle cost assessment of optimally designed reinforced concrete buildings under seismic actions. Reliab Eng Syst Saf 96:1311-1331
[42] Ohtori Y, Christenson RE, Spencer BF Jr, Dyke SJ (2004) Benchmark control problems for seismically excited nonlinear buildings. J Eng Mech 130(4):366-385
[43] Gupta A, Krawinkler H (1999) Seismic demands for performance evaluation of steel moment resisting frame structures. The John A. Blume Earthquake Engineering Center, Stanford University, Stanford, CA, Report No. 132
[44] Vamvatsikos D, Cornell CA (2002) Incremental dynamic analysis. Earthq Eng Struct Dyn 31(3):491-514
[45] Ghobarah A, Abou-Elfath H, Biddah A (1999) Response-based damage assessment of structures. Earthq Eng Struct Dyn 28(1):79-104
[46] FEMA-273 (1997) NEHRP guidelines for seismic rehabilitation of buildings. Washington DC - FEM
[47] Ghobarah A (2004) On drift limits associated with different damage levels, In: Proceedings of the International Workshop on Performance-Based Seismic Design – Concepts and Implementation, Bled, Slovenia 321-332
[48] FEMA-350 (2000) Recommended seismic design criteria for new steel moment-frame buildings. Washington DC - FEMA
[49] Lavan O (2017) Multi-objective optimal design of tuned mass dampers. Struct Control Health Monit e2008:1-16.
[50] Lin CC, Wang JF, Lien CH, Chiang HW, Lin CS (2010) Optimum design and experimental study of multiple tuned mass dampers with limited stroke. Earthq Eng Struct Dyn 39:1631-1651
[51] Daniel Y, Lavan O (2014) Gradient based optimal seismic retrofitting of 3D irregular buildings using multiple tuned mass dampers. Comput and Struct 139: 84-97